Engineering Geology 375 (2026) 109133



Contents lists available at ScienceDirect

Engineering Geology

journal homepage: www.elsevier.com/locate/enggeo

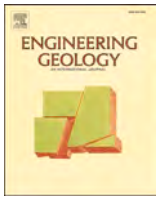

Borehole data and multiple geophysical methods for the characterization of a thick Quaternary succession in a synclinal setting of the active Ferrara Tectonic Arc (Italy)☆

Giuseppe Di Giulio [a,1], Marco Stefani [d], Giuliano Milana [a], Maurizio Vassallo [a], Sara Amoroso [c,a], Gabriele Tarabusi [a], Luca Baradello [b], Alessandro Affatato [b], Alfio Barbagallo [b], Stefano Maffione [b], Lorenzo Petronio [b,2], Luca Minarelli [a,*]

[a] Istituto Nazionale di Geofisica e Vulcanologia, INGV, Rome, Italy
[b] Istituto Nazionale di Oceanografia e di Geofisica Sperimentale, OGS, Trieste, Italy
[c] University of Chieti-Pescara, Department of Engineering and Geology, Pescara, Italy
[d] University of Ferrara, Department of Architecture, Ferrara, Italy

ARTICLE INFO

Keywords:
Borehole
Po Plain
Active and passive measurements
Shear-wave velocity
Stratigraphic units

ABSTRACT

Determining seismic velocities and bedrock depth in tectonically active sedimentary basins with thick unlithified successions remains challenging, due to the need for complex and costly geophysical and stratigraphic investigations. This study focuses on a test site in the southeastern Po Plain, where multiple geophysical and stratigraphic methods were applied to investigate a thick Quaternary sequence. The aim is to compare and evaluate different investigation approaches, and to characterize the seismic properties of the marine-to-continental stratigraphic succession accumulated in a synclinal setting of the active Ferrara Tectonic Arc. The sedimentary succession was drilled, cuttings were analyzed, and a natural gamma-ray log was acquired in the borehole. P- and S-wave velocity profiles were obtained in the well through down-hole tests, among the deepest available in the Po Plain. An active seismic reflection survey and passive seismic arrays were also acquired at the surface. Single-station ambient noise measurements were also carried out to detect site resonance frequencies and to estimate the main impedance contrasts. Consistent P- and S-wave velocity profiles were obtained from multiple seismic methods. Passive seismic data extended the interpretation below the borehole depth, revealing the deep seismic bedrock. The velocity data constrain characteristic values for most Quaternary units and define a power-law relationship between shear-wave velocity and depth. Major seismic reflectors were linked to regional stratigraphic discontinuities and correlated with observed resonance frequencies. These results provide a reference framework for analogous settings, supporting seismic interpretation and site-response assessment, where direct velocity data are unavailable. This study develops a novel interdisciplinary seismo-stratigraphic model exportable to analogous sectors of the Apennine foredeep basin.

1. Introduction

During earthquakes, deep sedimentary basins are typically affected by both ground-motion amplification and increase in shaking duration. It is well understood that such phenomena are tied to the reduction of the wave propagation velocity in the sediments and to the seismic waves trapping between the bedrock and the surface (e.g. Bard and Bouchon, 1985; Kagawa et al., 2004; Riga et al., 2016). Proper understanding of the local ground-motion amplification requires a good knowledge of the distribution of the wave velocity, of the nature of the stratigraphic units involved, and of the bedrock depth. This information is often missing in deep sedimentary basins with thick successions of unlithified sediments, where drilling may become costly and determination of the involved velocities is often achieved through less expensive indirect geophysical

☆ This article is part of a Special issue entitled: 'Geophysics to aid Geomodeling' published in Engineering Geology.
* Corresponding author.
[1] Giuseppe Di Giulio First author.
[2] Lorenzo Petronio passed away before this submission.

https://doi.org/10.1016/j.enggeo.2026.109133
Received 9 February 2026; Received in revised form 30 September 2026; Accepted 11 October 2026
Available online 12 October 2026
0013-7952/© 2026 The Authors. Published by Elsevier B.V. This is an open access article under the CC BY license (http://creativecommons.org/licenses/by/4.0/).

approaches. Very few case studies have indeed been reported worldwide in which velocities were directly measured down to depths of several hundred meters (e.g. Ohta et al., 1980) and linked to observed lithologies, because of the significant economic cost and the technical difficulty in performing a combined geophysical and geotechnical investigation. The seismic data acquired by hydrocarbon exploration are commonly not available to the scientific community and lack comprehensive velocity measurements at shallow depths. Indirect geophysical acquisition techniques at the surface are normally used to mend the lack of velocity data measured below some tens of meters. Passive techniques based on ambient vibrations, such as H/*V* (for horizontal-to-vertical noise spectral ratios; Nakamura, 2019) or array methods (Arai and Tokimatsu, 2005) provide velocity profile in deep basins, usually through a joint inversion of surface-wave data and fundamental frequencies. Similar approaches based on passive data inversion have been applied for the determination of deep Vs models in several regions worldwide, including the Mississippi Embayment (Himel and Wood, 2022; Rosenblad et al., 2010), New Zealand (Deschenes et al., 2018; Teague et al., 2018; Giallini et al., 2024) and in Kashmir valley (Gupta et al., 2023). Several authors (e.g., Ibs-von Seht and Wohlenberg, 1999; Comina et al., 2023) have developed empirical conversion relationships linking wavelength or site resonance frequency to bedrock depth, thereby providing insights into the Vs profile while reducing the need for a full inversion procedure. However, the effectiveness of passive non-invasive techniques is generally high in presence of a sharp seismic contrast occurring at a relatively shallow depth (about <200 m, Garofalo et al., 2016, Tarabusi et al., 2024). Conversely, the performance of passive methods tends to decrease with increasing bedrock depth and in the presence of weak seismic impedance contrasts (Bonnefoy-Claudet et al., 2006; Molnar et al., 2022).

In May 2012 a seismic sequence impacted the Po Plain, Italy, prompting an important geophysical research effort. Some of the contributions focused on the reconstruction of velocity profiles and bedrock depth (Milana et al., 2014; Mulargia and Castellaro, 2016; Mascandola et al., 2019; Mantovani et al., 2019; Petronio et al., 2023), the assessment of site amplification and ground motion prediction (Lanzano et al., 2016; Mascandola et al., 2021, 2023), and the modelling of seismic wave propagation (Molinari et al., 2015; Dujardin et al., 2016). However, the estimation of the shear-wave velocity in deep layers and the depth of the seismic bedrock is not completely resolved for the Po plain area. To obtain reliable velocity profiles at significant depths in complex geological settings, like the Po Plain, a multidisciplinary approach that combines different geophysical methodologies is highly recommended (Hunter et al., 2002; Arai and Tokimatsu, 2005; Woolery et al., 2016; Himel and Wood, 2021; Matsushima et al., 2024). In this framework, a multidisciplinary approach combining borehole investigations with active and passive seismic techniques was applied in this research to derive 1D velocity models for a syncline test site located in the southeastern Po Plain, southwest of Ferrara. The research site was selected because it is located within the epicentral area of the 2012 seismic sequence (Pondrelli et al., 2012), lies in the central sector of the Ferrara Tectonic Arc, where a substantial thickness of Quaternary sediments has been documented (Pieri and Groppi, 1981), and benefits from a previously conducted borehole survey (Minarelli et al., 2016) that provided compressional (Vp) and shear-wave (Vs) velocity measurements down to a depth of 265 m.

The new investigation campaigns included the acquisition of P- and S-wave velocity profiles down to the depth of 365 m from down-hole test. In addition, an active seismic reflection survey and active and passive seismic arrays were acquired at the surface. The results of the seismic measurements were correlated with the subsurface stratigraphy derived from the borehole, calibrated using natural gamma ray log provided by the Veneto Region Geological Survey. Single-station ambient vibration recordings were also acquired and processed to compute horizontal-to-vertical (H/*V*) spectral ratios (Nakamura, 2019; Molnar et al., 2022). The aim was to investigate potential correlations between frequencies associated with identified seismic reflectors and peaks in the H/*V* spectral ratio curves. The new measurements and analyses significantly improve the understanding of the physico-mechanical properties of the stratigraphic succession, enabling the identification of a power-law relationship between Vs and depth, with seismic bedrock inferred at approximately 700 m. The velocity profiles and power-law relationships obtained in this study can be used as a reference and extrapolated to similar synclinal areas across the Po Basin for seismic profile interpretation, local seismic response assessment, and as initial models for inversion procedures where direct velocity measurements are not available.

2. Geological and stratigraphy framework

The research area belongs to the external part of the Apennine Chain, buried beneath the alluvial plain of the Po River, northern Italy. The compressive tectonic framework of the region is dominated by active thrust-fold structures (Martelli et al., 2016; Pieri and Groppi, 1981), developed through Plio-Pleistocene times (Ghielmi et al., 2013; Vannoli et al., 2015). The investigation site (Fig. 1) is placed within the two anticline belts of the Ferrara tectonic Arc, forming the most external portion of the buried chain (Pieri and Groppi, 1981). These inverse faults are active, as the earthquakes that struck the area in May 2012 demonstrate (Pondrelli et al., 2012). The active deformation largely influenced the Plio-Quaternary stratigraphic architecture of the area (Fig. 1).

The Quaternary evolution was also affected by large eustasy and climate fluctuations. The combination of these factors induced the unconformity surfaces supporting the subdivision of the sedimentary succession into allostratigraphic units, such as supersynthem, synthem, and subsynthem (Regione Emilia-Romagna, 1998). The geometry and depth of the main stratigraphic units and boundary surfaces were summarized by a three-dimensional structural model of central Emilia-Romagna (Klin et al., 2019), based on geological data and deep seismic lines and boreholes for hydrocarbon exploration. The discordance surfaces are well developed on the structural highs, whereas they become less sharp and grade into paraconformity toward the fast-subsiding syncline area (Fig. 1). The oldest unit described in this work consists of deep-water terrigenous turbidites, sedimented through Pliocene times ("inner" Porto Garibaldi Fm, Ghielmi et al., 2013). The turbidite unit top corresponds to the interruption of the sand sedimentation, induced by the tectonic rising of anticline submarine bulges preventing the turbidite currents from reaching the study area (Ghielmi et al., 2013). The following unit, known in the literature as "Marine Quaternary" (Martelli, 2021; Petronio et al., 2023), witnesses the Gelasian-Calabrian evolution, from deep water argillaceous environments to coastal-deltaic systems. In accordance with the present-day stratigraphic scale, we use the "long Quaternary" definition (Finney, 2010), incorporating the Gelasian, a use that must be considered while comparing this contribution with the previous literature.

A phase of deformation and local erosion on the tectonic highs induced an unconformity surface, marking the boundary between the Marine Quaternary and the overlaying Emilia-Romagna Supersynthem (Martelli, 2021). The latter is bipartite into Lower (AEI) and Upper (AES) Emilia-Romagna Synthems (Fig. 1) by a younger gentler discordance surface.

At the study site, AEI Synthem still often records marine environments. The marine and brackish influences vanish upward, in the lower portion of the AES Synthem. The upper portion of AES records purely continental environments (Minarelli et al., 2016). The synthems, in turn, frame a number of subsynthems, each recording a climatic and glacio-eustatic fluctuation, developed in the 100,000 year frequency band (Regione Emilia-Romagna, 1998). In the continental successions, the base of each subsynthem records the deactivation of the middle alluvial plain, coarse-grained synglacial sedimentation. Continental *syn*-transgressive units are capped by organic-rich mud, deposited into lower alluvial plain and marsh settings. The regressive trend of the following alluvial plain successions climaxes into new intervals of synglacial sands (Cibin and Segadelli, 2009).

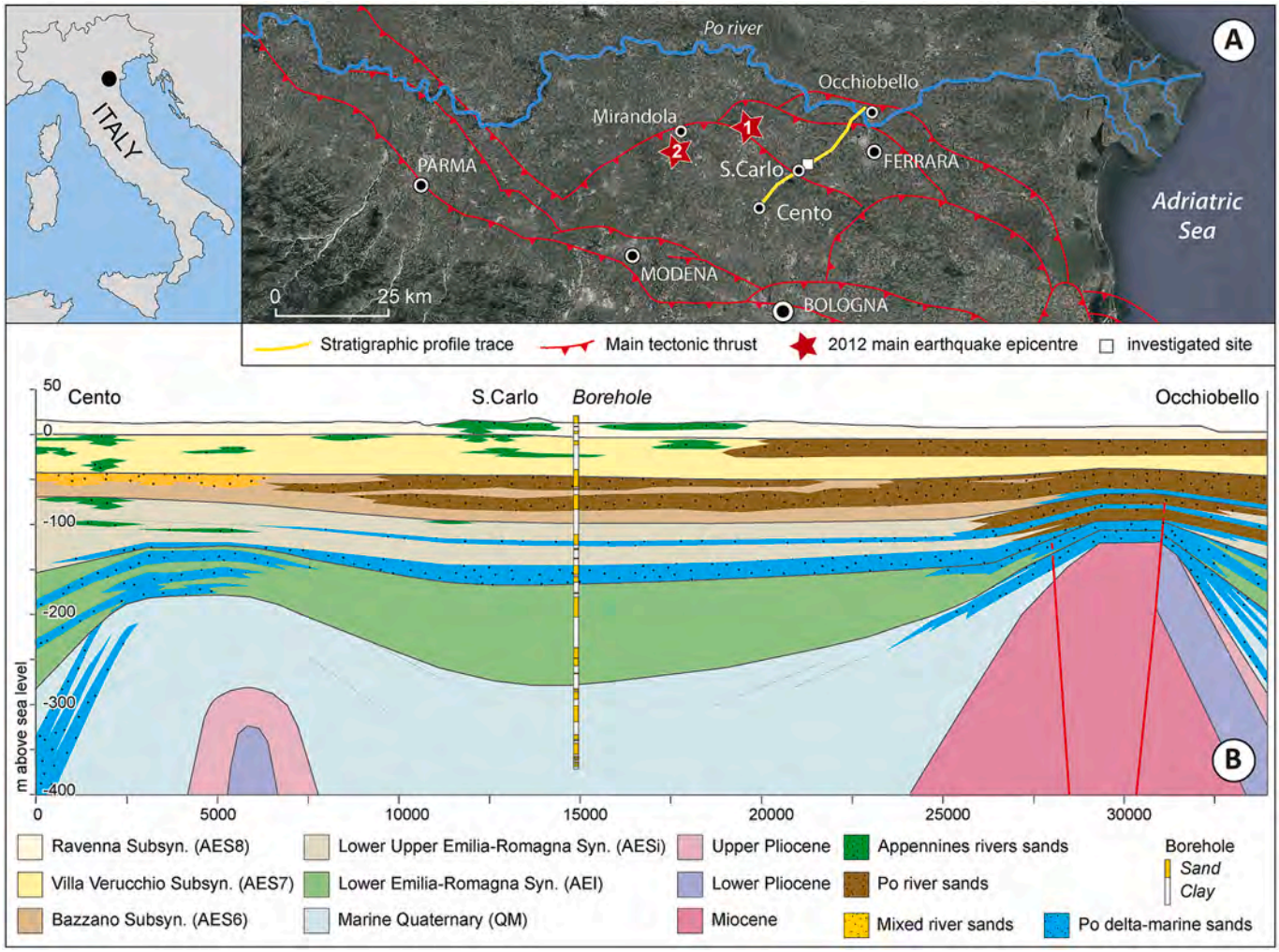

Fig. 1. Geological and seismotectonic framework of the studied Quaternary stratigraphic succession. The borehole investigated by down-hole measurements crosses a Quaternary succession deposited into an active synclinal structure near Ferrara. Modified from Minarelli et al. (2016).

3. Seismic surveys

Geophysical data were collected in the study area (Fig. 2) using active and passive seismic survey techniques to obtain velocity profiles of the deep subsurface. Active seismic methods, commonly used in geophysical prospecting and deep subsurface hydrocarbon exploration, were combined to passive techniques based on surface waves, which are widely used in seismic microzonation and site effect studies.

Table 1 summarizes the investigation techniques, configurations and processing used for velocity profiles and resonance frequency assessment. The active seismic surveys involved multiple energy sources, including a hammer and a MiniGun for the generation of compressional (P-) waves, as well as a MiniVib vibratory truck operating in shear-wave mode (S-waves) with a linear up-sweep. Down-hole tests provided some of the deepest available shear-wave (Vs) and compressional-wave (Vp) velocity profiles in the Po Plain. These results were compared with previous measurements acquired in the same borehole (Minarelli et al., 2016). At the surface, 80 single-component horizontal (SH) geophones were deployed along a linear array (Fig. 2) to record reflected wavefields generated by the MiniVib source. The same source was also used to energize a 1D linear array of 72 horizontal geophones, with the recorded data analyzed using the frequency–wavenumber (F—K) technique. Passive seismic data were acquired through measurements of ambient vibrations recorded by different configurations, including a 1D linear array of 72 horizontal geophones, a 2D array of 14 seismic stations with a maximum aperture of approximately 880 m, and single-station measurements (Fig. 2). The H/*V* measurements were used to investigate potential correlations between major reflectors identified in the seismic data and the observed H/*V* spectral peaks.

3.1. SH-wave borehole measurements

Shear waves (SH) were generated using a vibrating MiniVib truck, with a 16 s linear up-sweep, and recorded in the borehole down to a depth of 365 m, using a three-component (3C) borehole geophone (Table 1). Measurements were acquired at 2 m spacing along the interval overlapping with previous investigations (Minarelli et al., 2016), whereas a 1 m spacing was adopted for the underlying deeper portion. To compute the shear-wave velocity, the data acquired in the borehole (Fig. A1 in the Appendix material) were processed through a sequence of steps aimed at enhancing signal quality and improving the reliability of the velocity estimation. A cross-correlation procedure was applied using the Ground Force pilot signal, while simultaneously adjusting the acquisition parameters stored in the data header. Subsequently, a hodogram analysis was performed, involving the rotation of the signals recorded by the borehole geophone along the horizontal components (H1 and H2), in order to obtain the Hmax and Hmin components. In this configuration, Hmax corresponds to the receiver–source plane and represents the direction of maximum energy, whereas Hmin identifies the orthogonal direction characterized by minimum energy. The dataset

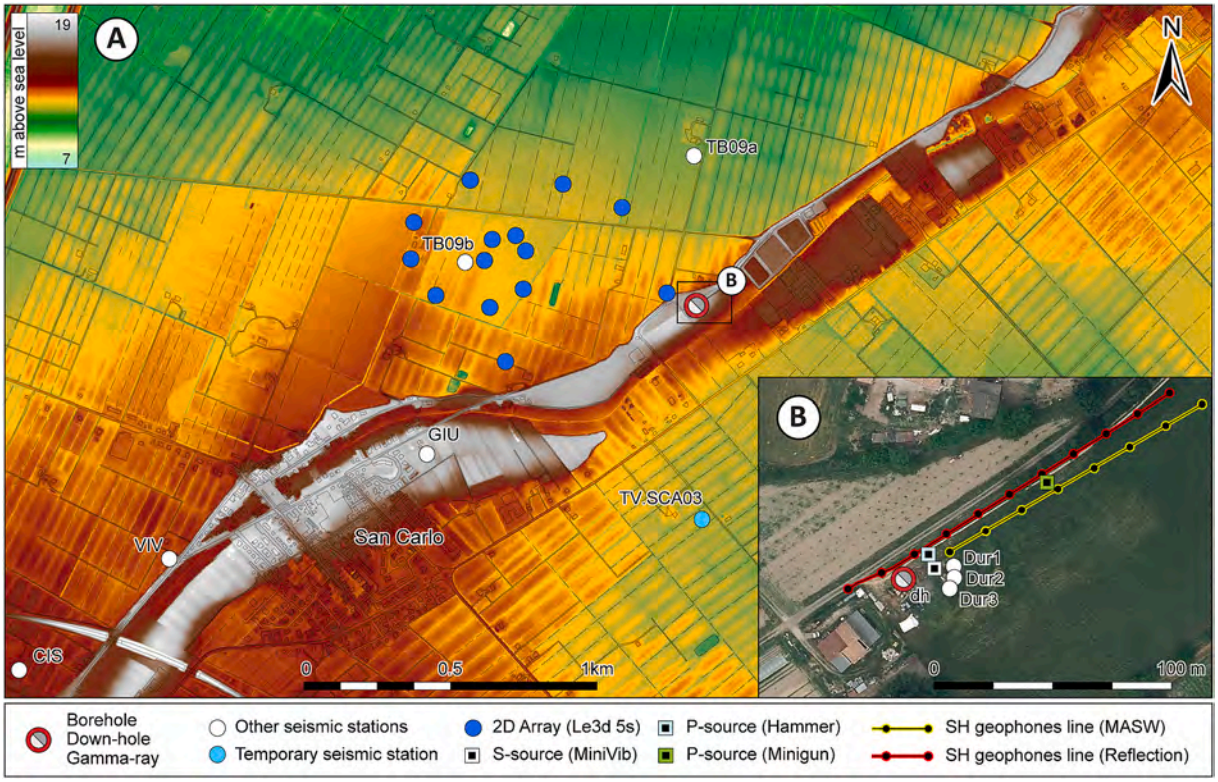

Fig. 2. (A) Base map showing the topography and digital elevation model, with the locations of the different types of geophysical investigations. (B) Satellite image showing a detailed view of the investigated borehole area and the layout of the linear seismic arrays at the surface.

was then processed to remove tube-wave effects through F-K filtering. To further enhance the signal generated by the sweep, an Ormsby band-pass filter with corner frequencies of 10–20–120–140 Hz was applied. The direct arrivals were subsequently picked, averaging over five adjacent traces in order to reduce picking instability and improve consistency. The analysis of the two SH sweeps generated by the vibroseis at the same location, but with opposite signal direction, shows consistent polarity in the correlated signals and improved data quality. The high quality of the seismic records is evident in Fig. 3, where coherent linear events associated with waves reflected by the main seismic impedance contrasts can be clearly observed. Three predictive deep reflectors were clearly identified (red markers in Fig. 3) by considering the intersection points between the reflected events and the direct waves, using the methodology proposed by Godio and Strobbia (2007). The projection of these intersections onto the X-axis provided an approximate estimate of the interface depths at 163 m, 243 m, and 292 m. Finally, to perform the time-to-depth conversion, velocity profiles were calculated as interval velocities smoothed over five measurement values.

3.2. P-wave borehole measurements

To acquire P-wave data in the well, both an impulsive hammer and a Minigun Isotta source were used. The hammer source-well offset was 14 m and the Minigun one 75 m (square symbols in Fig. 2B). To assess the effectiveness of the two source types, separate acquisitions were performed. The hammer source yielded a low signal-to-noise ratio at greater depths; therefore, only the data acquired with the minigun were used to determine the Vp profile. The P-wave acquisition using the 115 m BayCable consisted of three main deployment depth intervals (300–181 m, 180–61 m, and 60–13 m). The cable was equipped with 24 hydrophones with a 5-m inter-trace spacing. During each acquisition step, the cable was progressively raised across five shifted positions, with a 1-m offset.

The processing workflow was the same as that adopted for the S-wave analysis, except for the lack of crosscorrelation, the absence of component rotation, and the application of a different 10–20–160–200 Hz Ormsby filter. This method provided direct Vp measurements in the borehole over the depth interval between 13 and 300 m with measurements at 1 m depth intervals. Water was encountered in the borehole at a depth of 9.2 m. The Vp values ranging between 1600 and 1900 m/s indicate water-saturated sediments along the entire profile.

3.3. SH-wave reflection measurements

Using the same MiniVib source together with a 158 m long geophones line at the surface (Fig. 2B), a reflection shot was also performed. The acquisition configuration is summarized in Table 1. Velocity analysis was carried out on a common-shot gather using semblance analysis (Fig. 4), providing an independent estimate of the Vs model. Several reflections are visible in the results (orange arrows in Fig. 4). The semblance peaks (Fig. 4) correspond to the velocities providing the best normal moveout (NMO) correction for stacking. Stack velocities were converted into interval velocities using the formula proposed by Dix (1955). The Vs model was then compared with direct down-hole Vs measurements, assuming a horizontally layered subsurface, a reasonable assumption given the stratigraphic framework of the investigated depth interval at the test site.

3.4. 2D Passive array at the surface

A 2D passive array consisting of 14 seismic stations was deployed in a spiral-like geometry, with a minimum inter-station distance of about 60 m and a maximum aperture of 880 m. The center of the 2D array was located approximately 700 m from the borehole site (Fig. 2A). The array recorded passive seismic data at a sampling rate of 250 Hz over a time interval longer than 3 h (Table 1). Each station was equipped with a 24-bit digitizer (Reftek130) coupled with a three-component medium-

Table 1
Seismic surveys applied in this study.

Survey	Source	Receiver	Acquisition	Geometry	Processing	Output
SH-wave (borehole)	MiniVib T2500 IVI (sweep 10–120 Hz; time-length 16 s)	Borehole 3C sensor Geostuff BHG-2 (15 Hz)	DaqLink III, 0.0625 ms sampling, 2 2 s correlated-record window (for SH) beyond the 16-s sweep	0–365 m depth (2 m step, 0–265 m) (1 m step, 265–365 m)	First-break picking	Vs profile
P-wave (borehole)	Isotta MiniGun and Hammer	24 hydrophone string, 5 m spacing Geotomographie AQ200 (1 Hz–15 KHz)	DaqLink III, 0.0625 ms sampling	13–300 depth (1 m step)	First-break picking	Vp profile
SH-reflection (surface)	MiniVib T2500 IVI (sweep 10–120 Hz; time-length 16 s)	80 SH geophones LGT-20D (40 Hz)	SUMMIT II DMT, 0.5 ms sampling, 2 s time window	158 m line (2 m spacing)	Semblance analysis (Dix formula)	Vs profile
2D Passive array (surface)	Ambient Vibration	14 velocimeters 3C Le3D/5s	Reftek130 (Le3D/5s), sampling 250 Hz,3 hours recording	Spiral array (880 m aperture)	Surface-wave analysis (F-K + SPAC; low frequency), Inversion of dispersion curves	Vs profile
1D Linear array (surface)	Active MiniVib T2500 IVI (sweep 10–120 Hz; duration 16 s)	72 SH geophones Geospace GS11-D (4.5 Hz)	3 multi-channel systems (Geometric Geode), sampling 2000 Hz, 32 record – 20 s each	linear array 124 m (1 to 3 m spacing)	Surface-wave analysis (F-K; high frequency), Inversion of dispersion curves	Vs profile
1D Linear array (surface)	Passive Ambient Vibration	72 SH geophones Geospace GS11-D (4.5 Hz)	3 multi-channel systems Geometric Geode, sampling 250 Hz, 32 min. recording	linear array 124 m (1 to 3 m spacing)	Surface-wave analysis (F-K; high frequency), Inversion of dispersion curves	Vs profile
H/V measurements (surface)	Ambient Vibration (Standard)	Velocimeters 3C Le3D/5s; Velocimeters 3C Sara Electronics - 2 Hz	Standard acquisition. Reftek130 (Le3D/5s), Sara Datalogger (2 Hz), sampling 250 Hz,some hours	Single station	H/V analysis	Resonance frequency
H/V measurements (surface)	Ambient Vibration (Continuous)	Velocimeters 3C Le3D/5s	Continuous acquisition. Reftek130 (Le3D/5s), 45 days - TV.SCA03	Single station	H/V analysis	Resonance frequency

period Lennartz velocimeter (Le3d5s, eigenfrequency 0.2 Hz). Time synchronization was ensured by GPS antennas installed at each station, while accurate station locations were obtained using a Leica GNSS antenna, providing centimetric precision. Array processing was done using Geopsy software (http://www.geopsy.org; Wathelet et al., 2018, 2020).

Three-component data from the 2D array were processed using the high-resolution Rayleigh beamforming (RTBF) method implemented in Geopsy. RTBF analyzes vertical and radial components by searching F-K maxima in the wavenumber domain (kx, ky), and separates Rayleigh and Love wave contributions by maximizing at high resolution beam power. The method also evaluates the sign of the ellipticity angle, which indicates retrograde (negative) or prograde (positive) Rayleigh-wave particle motion.

The results of the 2D array analysis are shown in Fig. A2 (in the Appendix) for Rayleigh and Love waves. The Rayleigh-wave analysis shows two distinct dispersion curves (Fig. A2A and A2B) associated with

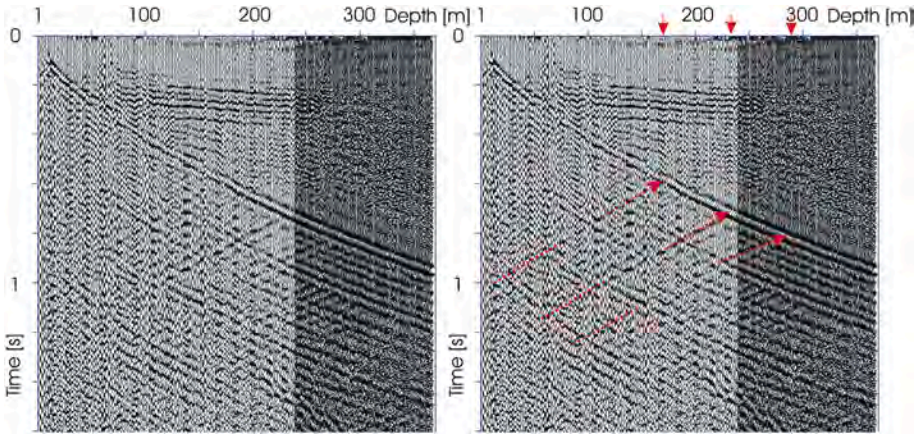

Fig. 3. SH borehole data shown in one-way-time representation (left) and with interpretation (right). The horizontal axe indicates the depth of the hole, the vertical axe indicates the one-way travel time. The traces are spaced every 2 m in the upper part and every 1 m in the deeper part. Key reflected signals are highlighted with red dotted lines. Intersections between reflected signals (coherent, linear event) and direct waves are indicated by red arrows, with the upper arrows denoting estimated depths of 163 m, 243 m, and 292 m. (For interpretation of the references to colour in this figure legend, the reader is referred to the web version of this article.)

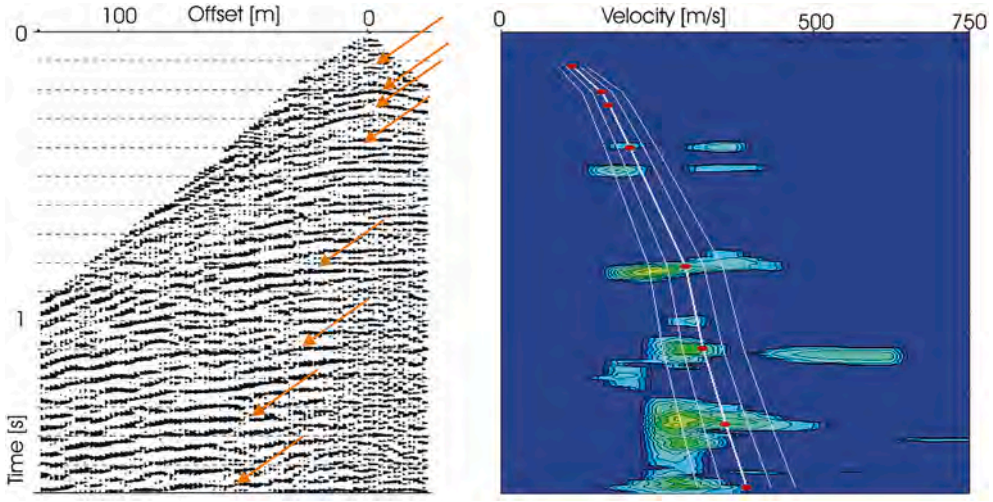

Fig. 4. S-wave common shot gather (left) acquired at the surface and its semblance (right). The time axe is represented in two-way travel time (twt). In the right panel, dark blue indicates low coherence, while yellow indicates high coherence. The red picks indicate the stack velocity values associated with the best normal moveout (NMO) correction of reflections. The other lines represent four guide functions (+ − 5% and + −10%). In the left panel, the orange arrows indicate the reflections at the peaks in semblance. (For interpretation of the references to colour in this figure legend, the reader is referred to the web version of this article.)

the fundamental (R0) and first higher mode (R1). The signed ellipticity associated with R0 is not well defined (Fig. A2C), whereas that associated with the R1 mode is more clearly resolved between 0.7 and 2 Hz (Fig. A2D). The Love-wave dispersion curve is also well resolved (Fig. A2E) from 0.5 to 2 Hz, with apparent velocities spanning from 500 to 180 m/s.

Vertical-component signals, acquired by the 2D array, were also processed using the Spatial Autocorrelation Analysis (SPAC; Aki, 1957), as implemented in Geopsy for irregular array geometries (Bettig et al., 2001). Dispersion curves were obtained from spatial autocorrelation coefficients azimuthally averaged within concentric rings of increasing radius, ensuring adequate inter-station spacing coverage (Fig. A3). Assuming a stationary microtremor field and a spatially homogeneous source distribution, the SPAC method is particularly effective at low frequencies, where it provides higher resolution than the F-K approach (Ohori et al., 2002; Okada, 2006).

SPAC analysis suggests the presence of Rayleigh waves below 1.5 Hz. The final selected dispersion curve spans the 0.4–1 Hz frequency range (Fig. A3). Phase velocities range from approximately 1000 to 400 m/s between 0.4 and 1 Hz.

3.5. 1D Linear array of geophones at the surface

A 1D linear array of 72 horizontal geophones (4.5 Hz eigenfrequency), spanning 124 m, was deployed at the surface (Fig. 2B). The array was used to record the SH-wave component during both active seismic acquisitions, performed using a MiniVib source, and passive ambient vibration measurements (Table 1). An example of recording, from three geophones located at the beginning, middle, and end of the line, is shown in Fig. A4 of the Appendix. The data were processed using approaches commonly known as multichannel analysis of surface waves (MASW; Park et al., 1999) and refraction microtremor (ReMi; Louie et al., 2022).

Conventional F-K analysis applied to the active data provided dispersion curves (Fig. A5 panel A in the Appendix), with apparent phase velocities ranging between 190 and 130 m/s over the 4–50 Hz frequency band. Using the same line of horizontal geophones, a F-K analysis was performed also on the passive data (Fig. A5 panel B). Given the alignment of the MiniVib source with the linear array, the maxima of the beam spectra were picked in the velocity–frequency domain, in the active data analysis. In the passive data analysis, the minimum velocity envelope was picked (Fig. A5B) according to Louie et al. (2022), since ambient vibrations are predominantly composed of surface waves and the wavefield is not usually unidirectional. The good agreement between the dispersion curves of both active and passive data (Fig. A5 panel C), suggests that Love-wave dispersion is also present in the passive data. As expected, the passive data performs better than the active ones in recovering information from the lower frequency range (Stephenson et al., 2005; Boore and Asten, 2008).

3.6. H/V measurements

To detect the resonant frequencies and to assess their temporal stability, H/V noise spectral ratios were calculated from long records of single-station ambient vibrations acquired repeatedly over multiple days and years by different seismic stations nearby the borehole. This approach was adopted since the Po Plain basin is characterized by intense anthropogenic vibrations and low-frequency resonances (Massa et al., 2022), therefore long acquisition times and repeated measurements are preferable here to reliably identify the resonance frequencies. The acquisitions were performed close to the borehole and in the surrounding area, within a 3 km distance (Fig. 2), in order to also assess the spatial homogeneity of the H/V curves and, consequently, of the investigated subsurface stratigraphy.

To better identify the low-frequency peaks, several long-duration ambient noise measurements were carried out (Fig. 2A and Table 2). Some of these measurements were performed at night in order to assess the effect of reduced anthropogenic noise. The corresponding H/V spectral ratios were computed for all measurements. The same procedure was also applied to each station of the 2D array. The comparison of some of these measurements (Fig. 5) with the one performed at the borehole site (Dur2) reveals a consistent and homogeneous pattern of multiple weak peaks, likely connected to distinct seismic interfaces. Peaks below 1 Hz are recognizable in the directional H/V plots (Fig. 5), which show no significant azimuthal dependence, suggesting an absence of 2D or 3D site effects (Matsushima et al., 2017).

To verify the temporal stability of the H/V ratio, the ambient vibration data from a temporary seismic station (TV.SCA03 – https://eida.ingv.it/en/station/TV/SCA03), continuously recording over 45 days during the 2012 seismic sequence, were also analyzed (Fig. 2, Table 2). This station was equipped with the same sensor type (Le3d5s) and digitizer (Reftek digitizer) used in many of the other measurements. The H/V noise ratios at TV.SCA03 were processed and daily averaged using the HVNEA tool (Vassallo et al., 2023), which is particularly suitable for

Table 2
Summary of noise measurements and their technical characteristics. The measurement locations are shown in Fig. 2.

Name	Equipment	Date and time	Location
2D array (14 stations)	Reftek130 - datalogger Le3d5s - velocimeter	July 6, 2016 10:00 a.m. – 12:40 p.m.	Central station about 700 m from the borehole
Dur1	Sara SL06 2 Hz both a digitizer and recorder	January 10, 2016 9:30 a.m. – 2:30 p.m.	At the borehole
Dur2	Reftek130 - datalogger Le3d5s - velocimeter	November 26, 2018 10:00 p.m. – 5:00 a.m.	At the borehole
Dur3	Sara SL06 2 Hz both a digitizer and recorder	April 04, 2020 10:00 p.m. – 5:00 a.m.	At the borehole
GIU, VIV, CIS	Reftek130 - datalogger Le3d5s - velocimeter	November 26, 2018 10:00 p.m. – 5:00 a.m.	About 1 km, 2.5 km and 3 km south-west of the borehole
TB09a	Sara Terrabot 4.5 Hz both a digitizer and recorder	March 19, 2025 10:00 p.m. – 5:00 a.m.	About 500 m north from the borehole
TB09b	Sara Terrabot 4.5 Hz both a digitizer and recorder	March 19, 2025 10:00 p.m. – 5:00 a.m.	At the center of the 2D array
TV.SCA03	Reftek130 - datalogger Le3d5s - velocimeter	31 May - 15 July 2012 (45 days)	About 700 m south of the borehole

automatic processing of long-term time-series.

3.7. Dispersion curves and Inverted models

The surface-wave analyses described above resulted in the five dispersion curves shown in Fig. 6. All curves were obtained by resampling manually picked dispersion data. Dispersion curves derived from the different techniques exhibit consistent trends for the same wave types and modal orders, allowing the curves combination over a broad frequency range: 0.4–2 Hz for R0, 0.65–45 Hz for L0, and 0.8–2 Hz for R1. Dispersion curves above 3 Hz were derived from the analysis of the linear-array, whereas those below 3 Hz were obtained from processing the 2D-array data. The dispersion curve extending to the lowest frequencies was derived from the SPAC analysis, due to its greater capability to resolve longer wavelengths. The SPAC curve, characterized by an apparent velocity of approximately 1000 m/s at 0.4 Hz (Fig. 6), provides a maximum wavelength of about 2500 m within the R0 mode. Assuming an investigation depth approximately equal to one-third of the maximum wavelength, according to the commonly adopted empirical criterion, the surface-wave methods are expected to achieve an investigation depth of approximately 800 m.

The experimental dispersion curves show a gap within the frequency ranges of 2–3.5 Hz for Love waves and 0.8–1.2 Hz for Rayleigh waves as these intervals fall outside the theoretical resolution limits of the array geometries adopted during field acquisition. Despite this discontinuity, the overall trend and consistency observed at the frequency boundaries suggest a substantial continuity between adjacent frequency bands can reasonably be assumed.

The R0, R1, and L0 curves shown in Fig. 6 were used as input for an inversion procedure aimed at deriving a one-dimensional S-wave velocity (Vs) profile based on the arrays data. An additional constraint in the joint inversion was provided by the signed ellipticity of the R1 mode in the 0.6–1.2 Hz frequency range, derived from the RTBF analysis (Fig. A2d of the Appendix). The inversion procedure was performed using the improved neighborhood algorithm implemented in Geopsy.

Several model-space parameterizations were tested during inversion, considering layered models characterized by homogeneous elastic properties within each layer and an increase in seismic velocity with depth. The inversion was carried out using the simplest parameterization capable of adequately reproducing the experimental observations. The preferred velocity models obtained from inversion are shown in Fig. 7 and were derived using four main layers overlying seismic bedrock, with an increase of Vs with depth assigned to each layer. For the model parameterization, the free parameters (P- and S-wave velocities and layer thickness) were allowed to vary over a relatively wide range (Table S1 - Appendix Material).

The inverted models (Fig. 7) yielded misfit values lower than 0.6, where the misfit quantifies the deviation between theoretical predictions and experimental observations. Confidence in the inversion results is supported by the use of multiple dispersion curves covering a wide frequency range, as well as by the good agreement between experimental and theoretical curves for both the fundamental and first higher Rayleigh modes (Fig. 7A-B) and the fundamental Love-wave mode (Fig. 7C). The unresolved signed R1 ellipticity below 0.6 Hz (Fig. 7D) is likely related to the combined effect of limited array aperture and attenuation of higher-mode energy. This low-frequency limitation is compensated by the dispersion information derived from the SPAC analysis, which inherently performs better at lower frequencies, extending down to 0.4 Hz.

The inversion results indicate a relatively gradual increase of Vs with depth, with comparatively low shear-wave velocity values (<1000 m/s) observed at least within the uppermost 700 m of the investigated subsurface (Fig. 7F).

4. Result and discussion

The analysis of borehole data, seismic reflection measurements, and surface-wave inversion provides a robust and coherent framework for characterizing the subsurface velocity structure of the study area. The combination of SH-wave and P-wave borehole data with independent geophysical methods yields consistent shear-wave (Vs) and compressional-wave (Vp) velocity trends down to several hundred meters depth. The agreement among the different datasets supports the reliability of the derived velocity models and their applicability to stratigraphic and geophysical interpretation. The discussion is organized into three main parts: (i) comparison of Vs profiles obtained from different geophysical methods, with emphasis on their consistency, depth trends, and seismic bedrock identification; (ii) correlation between stratigraphic units and geophysical properties (Vs and Vp) derived from borehole and regional data; and (iii) interpretation of seismic reflectors as major impedance contrasts and their relationship with stratigraphic discontinuities and layering of the subsurface.

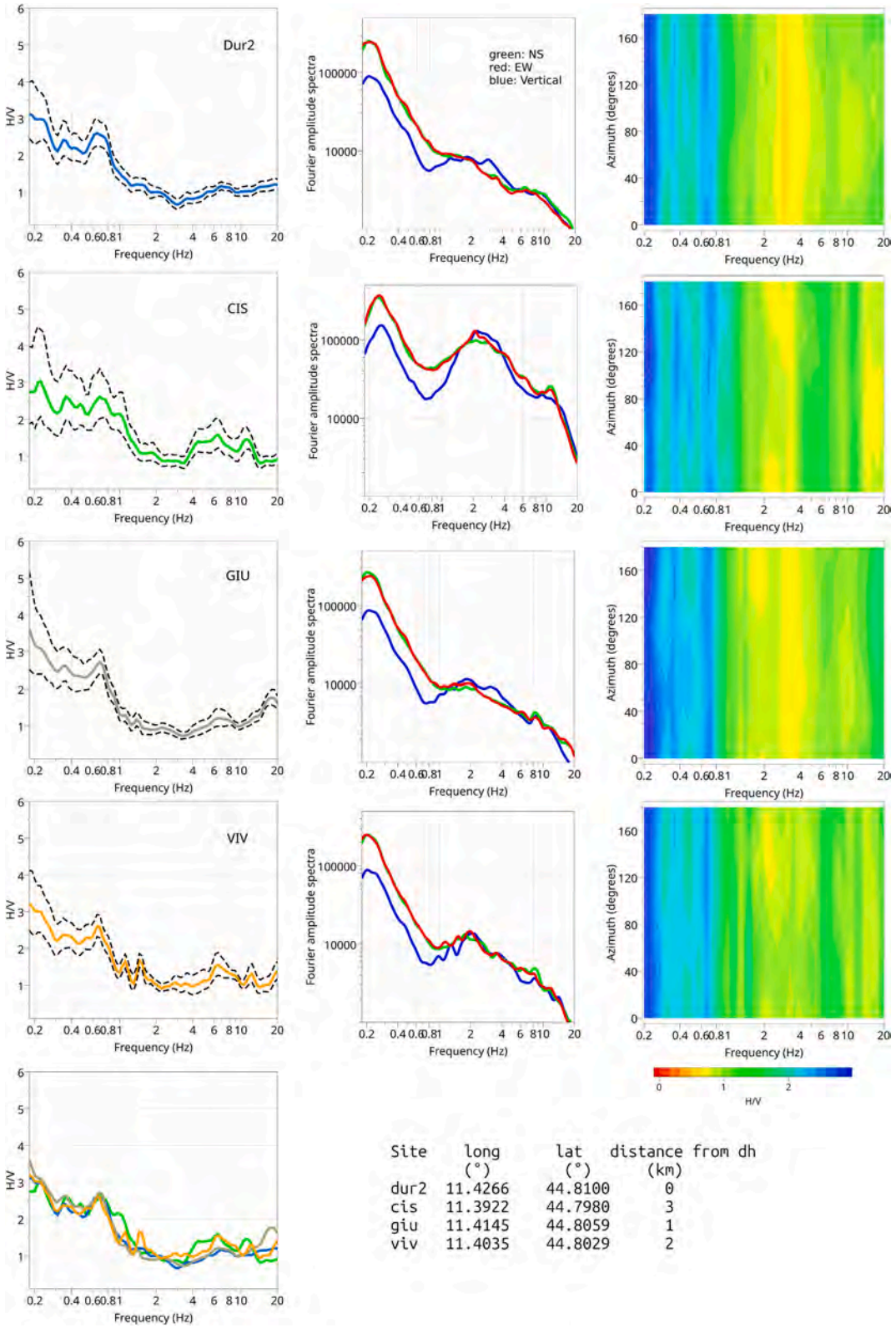

Fig. 5. H/V noise curves around the target site (Dur2 is located at the borehole) in the area of San Carlo village. All measurements were performed for an entire night (26–27 November 2018). H/V ratios, FAS of the three components (amplitude in arbitrary counts) and directional H/V analysis (with the colour scale representing H/V amplitude) are shown from left to right. The bottom panel shows the overlaying of the mean H/V curves. The coordinates of the measurements and their distance from the borehole site are also indicated. (For interpretation of the references to colour in this figure legend, the reader is referred to the web version of this article.)

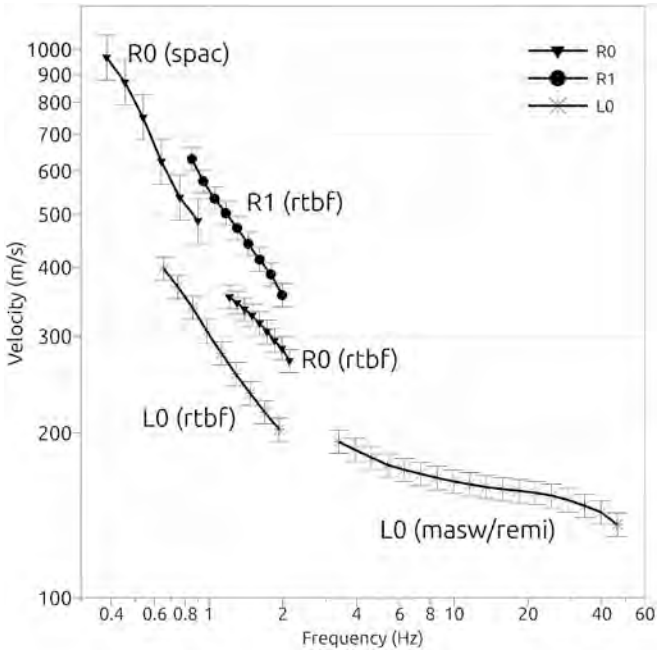

Fig. 6. Dispersion curves used for the inversion process. The method of analysis is described in brackets (see text). R0 and R1 stands for fundamental Rayleigh and first higher mode, L0 for fundamental Love wave. The vertical bars show the experimental uncertainty in the picking of the dispersion curves.

4.1. Velocity profiles

The analysis of data acquired through three independent geophysical techniques, i.e. down-hole measurements, seismic reflection surveys, and active and passive array recordings, yields mutually consistent Vs models, exhibiting similar spatial trends and velocity values (Fig. 8). Down-hole measurements allowed the reconstruction of a Vs profile down to 365 m and a Vp profile down to 300 m. The Vs profile exhibits a fluctuating trend, with a general increase in velocity, and therefore stiffness, with depth. The profile is punctuated by several intervals of sharp velocity increase. Weak fluctuations in the Vs values may have also been induced by the picking procedure. The other Vs profiles derived from seismic reflection and array analyses also show a general increase in velocity with depth. The reflection velocity model extends to about 300 m and the array best model to about 700 m (Fig. 8). The velocity models derived from all techniques indicate that, down to a depth of 365 m, Vs values remain significantly below the 800 m/s defining the engineering bedrock in both the European and Italian building codes (CEN, 2022; NTC18, 2018). The Vs profile derived from the surface-wave inversion of seismic array data reveals a marked increase in shear-wave velocity, with Vs values rising by approximately 400 m/s to exceeding 1200 m/s at a depth of about 700 m, suggesting the presence of a deep seismic bedrock. This interface corresponds to the most significant velocity contrast identified within the entire model. The discrepancies between velocity values obtained with the different methods can be quantified using the Coefficient of Variation (CoV), defined as the ratio of the standard deviation to the mean Vs as a function of depth (Garofalo et al., 2016). A comparison of down-hole, reflection, and surface-wave inversion data yields an average CoV of ~10% (Fig. 8).

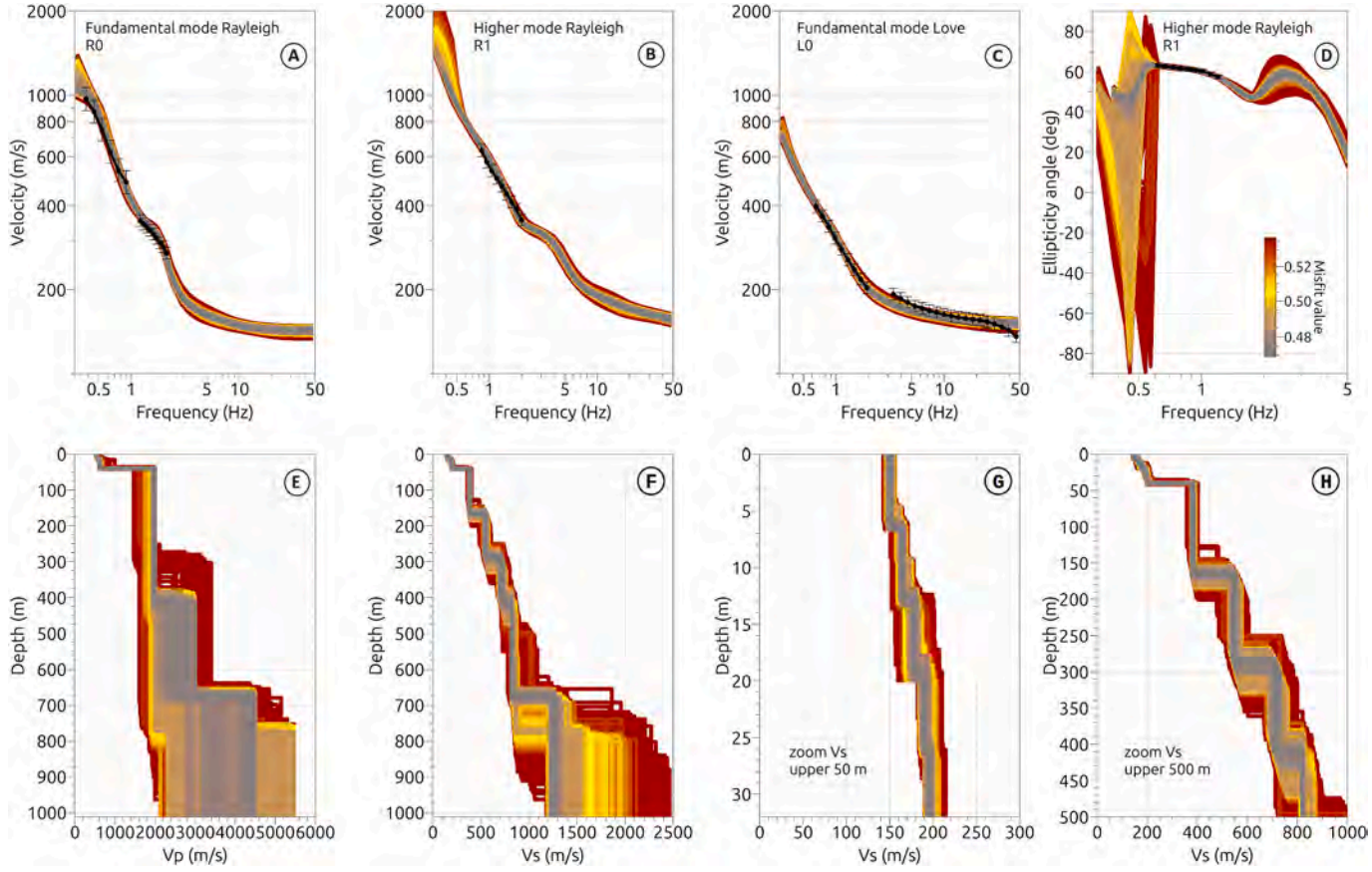

Fig. 7. Inversion results; the rainbow scale is proportional to the misfit value. The field data obtained from surveys are overlaid in black. A) DCs for the R0 mode. B) DCs for the R1 mode. C) DCs for the L0 mode. D) Signed ellipticity of the R1 mode. E) Vp inverted models. F) Vs inverted models. G) A zoomed view of the Vs inverted profile for the uppermost 30 m. H) A zoomed view of the Vs inverted profile for the first 500 m. (For interpretation of the references to colour in this figure legend, the reader is referred to the web version of this article.)

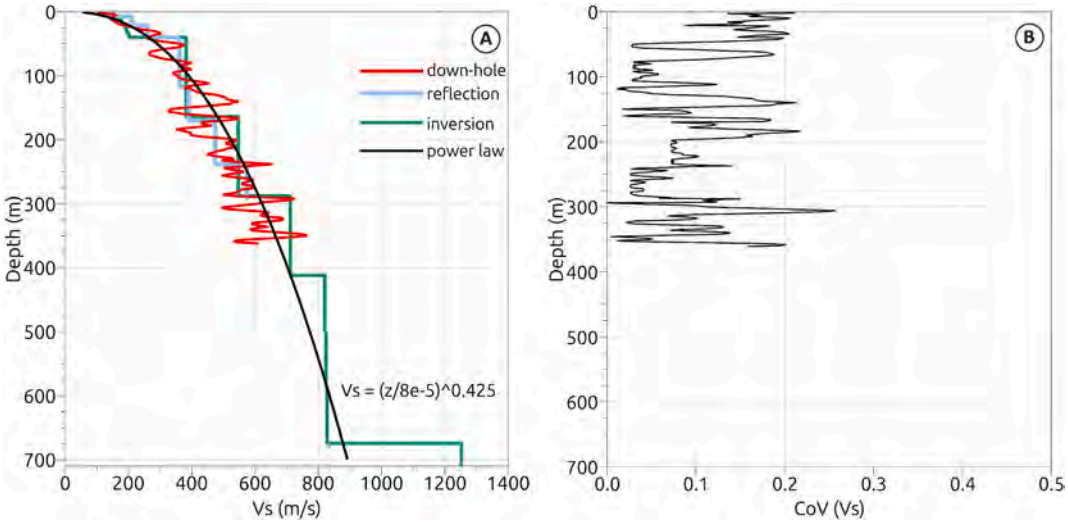

Fig. 8. Comparison of the Vs profiles. A) The Vs profiles from down-hole and reflection surveys are overlaid (as red and blue curves, respectively). The best-fitting model from the array inversion is also shown (in green). The power law function proposed in the main text is shown as a black curve. B) CoV (Coefficient of Variation) plot considering the Vs profiles obtained from borehole, reflection and inversion. Below 300 m, the Cov refers to the borehole and inversion profile. (For interpretation of the references to colour in this figure legend, the reader is referred to the web version of this article.)

The CoV rarely exceeds 20%, confirming the overall agreement among the methods and the reliability of the final models. Similar Vs velocity trends and values were documented in previous studies of the same stratigraphic interval (Minarelli et al., 2016; Petronio et al., 2023) providing additional support for the robustness of our velocity measurements. The agreement in shear-wave velocities between direct invasive geophysical surveys and non-invasive surface-wave array demonstrates the potential of the latter, when properly calibrated using direct data, for deep seismic characterization in analogous areas with thick sedimentary sequences. Based on the observed velocity profiles, a power-law function was defined to represent the mean velocity trend, expressed as $Vs = (z/a)^b$, where z indicates depth in meters (for $z > 4$ m), and the parameters a and b are 8×10^{-5} and 0.425, respectively (Fig. 8). For the uppermost 4 m, Vs was fixed at 100 m/s to avoid unrealistically low values. This power-law function can be used as a reference average profile for seismic response studies in similar geological settings of the Po Plain, after estimation of the bedrock depth, when deep Vs velocity profiles are not available.

The velocity profiles obtained from the down-hole survey were compared with previously acquired shallower measurements from the same borehole, published by Minarelli et al. (2016). A comparison of the shear-wave velocity measurements over the common depth interval of the first 265 m shows good agreement between the new and previous datasets (Fig. 9). The new survey, which extends the investigation depth to 365 m, provides novel information on the deeper section of the borehole, revealing a progressive increase in S-wave velocity with depth also in this interval (Fig. 9). The P-wave velocity profiles from the two down-hole surveys show substantial agreement in terms of both absolute values and general trends. Notably, both profiles exhibit a significant decrease in Vp values below 250 m depth, likely associated with the presence of biogenic methane occurring in both dissolved and free-gas phases, which induces partial pore-space saturation in the sediments. Similar conditions have been documented in other sectors of the basin of Po Valley and northern Adriatic (Ferrante et al., 2022). The Vp model derived from the inversion of the dispersion curves, however, shows significant differences from the down-hole profiles, particularly within the upper 40 m of the subsurface (Fig. 9). These differences may partly reflect the lower sensitivity of surface-wave dispersion data to Vp, particularly at shallow depths. In addition, the inherent non-uniqueness of the inversion, which was performed without imposing prior constraints on the initial parameterization (Table S1 in the Appendix), results in greater uncertainty in the inverted Vp model compared with the down-hole profiles.

4.2. Stratigraphic units and geophysical properties

The combined information from drilling, gamma-ray logging and seismic data, correlated with the regional geological framework (Cibin and Segadelli, 2009) enabled the identification of regional stratigraphic units at the research site and their correlation with the measured geophysical properties. The stratigraphic succession shows significant variations in geological and physical properties, reflecting changes in depositional dynamics, lithology, degree of stiffness, and fluid contents (Fig. 9). The obtained velocity profiles (Fig. 9) exhibit a good correlation with the subsurface stratigraphy. A summary of the geophysical properties of the identified stratigraphic units, including depth, thickness, Vp and Vs velocities from down-hole, seismic reflection, and array surveys, and gamma-ray log values is provided in Table 3.

In the following sections, the stratigraphic units are described in hierarchical order, from the uppermost Holocene continental deposits to the Pliocene deeper marine successions, highlighting their lithological characteristics and geophysical signatures.

4.2.1. Upper Emilia-Romagna Synthem (AES)

The AES unit frames the upper 162 m of the succession, and globally records a regressive evolution, from marginal marine to purely continental environments, periodically subject to synglacial lowstand conditions. The interval is organized into several subsynthems.

The Ravenna Subsynthem (AES8) is formed by Holocene sediments, found from the surface to 22 m of depth. The uppermost silty-sand body was deposited by the river Reno, during the 16th and 17th centuries A.D. (Caputo et al., 2016). The natural gamma ray log values of the granular sediments of AES8 generally fluctuate between 40 and 50 counts per second (c.p.s), values commonly found also in the fluvial sand within the underlying stratigraphic units (Fig. 9). The central portion of AES8 is formed by organic-rich muds, sedimented into an interfluvial depression and characterized by low seismic velocities, with average Vs values at about 150 m/s, but locally as low as 115 m/s. The lower portion of the unit consists of pedogenized continental silts, with carbonate concretions, older than 5000 years (Stefani et al., 2018), and showing comparatively higher Vs values, reaching 220 m/s.

The Villa Verucchio Subsynthem (AES7), between 22 and 58 m,

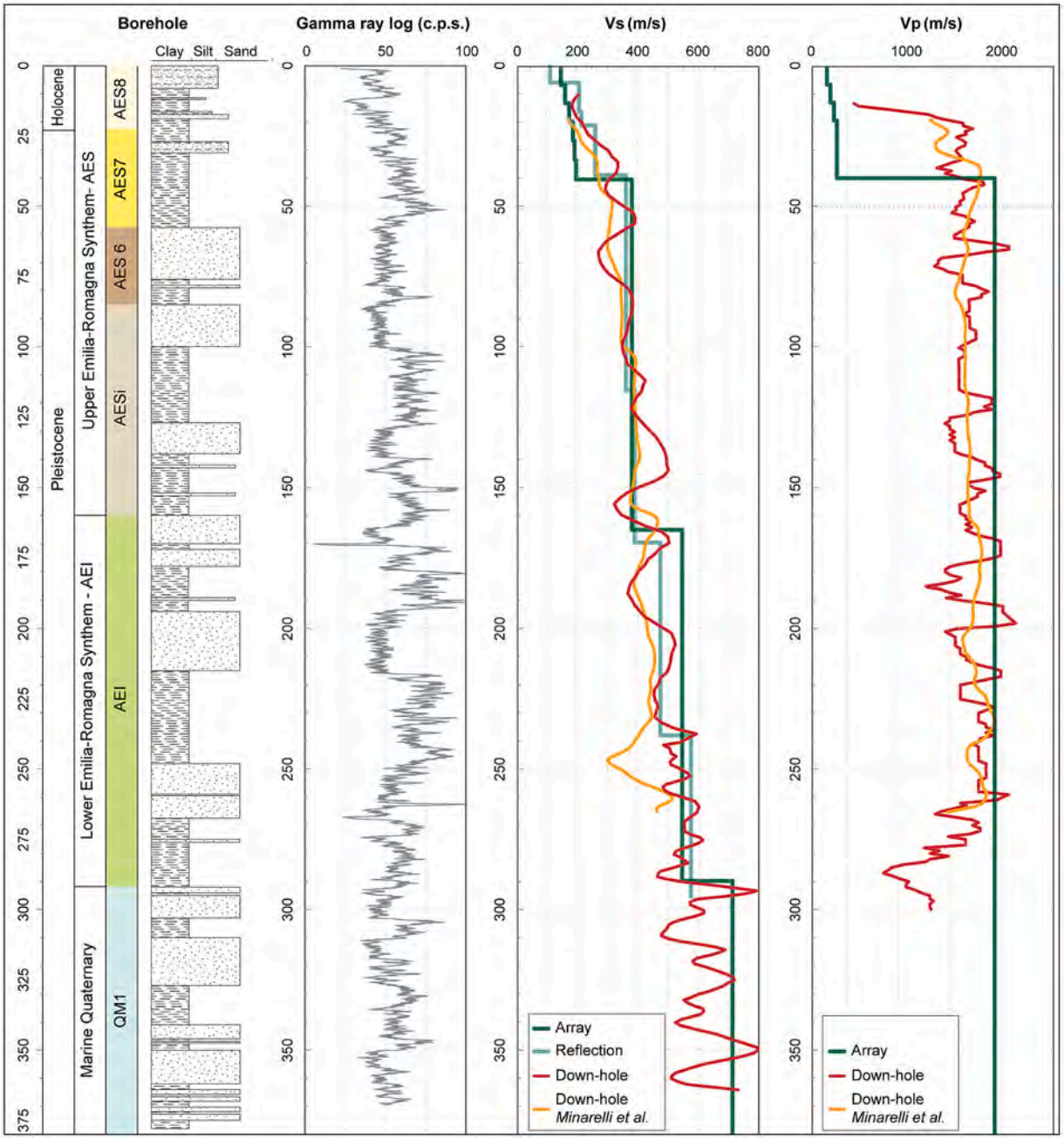

Fig. 9. Stratigraphic interpretation of the borehole, shown alongside the natural gamma-ray log, the shear-wave (Vs, red) and compressional-wave (Vp, red) velocity profiles from the down-hole. In orange, the previous down-hole profiles (Minarelli et al., 2016) are shown. In light green the Vs profile derived from seismic reflection, in green the Vs and Vp profile derived from the inversion of dispersion curves from array data.

Table 3
Stratigraphic units identified in the subsurface and corresponding geophysical parameters, including unit depth, thickness, P-wave velocity (Vp), S-wave velocity (Vs) obtained from down-hole, seismic reflection, array surveys (best fit model), and gamma-ray log recording.

Unit	Depth (m)	Thickness (m)	Down-hole Vp (m/s)	Down-hole Vs (m/s)	Reflection Vs (m/s)	Array Vs (m/s)	Gamma log (c.p.s.)
AES8	0–22	22	601–1703	140–225	114–217	150–190	23–60
AES7	22–58	36	1357–1813	225–390	260–362	190–382	40–88
AES6	58–85	27	1333–2057	270–382	362–362	382–382	39–80
AESi	85–162	77	1434–1968	322–500	362–390	382–382	35–95
AEI	162–292	130	836–2121	367–645	390–575	382–547	5–100
QM1	292–410	118	–	476–794	–	711–711	33–87
QM2	410–675	265	–	–	–	711–828	–
P2	675 -?	–	–	–	–	828–1252	–

records late Pleistocene continental environments and is rich in argillaceous sediments, with subordinated fluvial sand intercalations, sedimented by rivers outflowing the Apennines, particularly abundant in its upper synglacial portion (Stefani et al., 2018). The lower part of the unit, between 48 and 58 m, shows higher natural gamma ray log values, fluctuating between 75 and 85 c.p.s., associated with levels enriched in continental organic matter. The subsynthem top surface is marked by an increase of the Vs values, and a further increase was detected in the lower portion of the unit, with values in the range of 350–390 m/s, probably associated with pedogenized layers.

The upper Middle Pleistocene Bazzano Subsynthem (AES6), between 58 and 85 m, shows coarser-grained sediments, dominated by thick fluvial sand bodies accumulated by the Po River (Cibin and Segadelli, 2009), mainly during synglacial times. Finer-grained deposits form the lower part of the unit show levels exceeding 75 gamma-ray c.p.s. The borehole Vs measured in the alluvial sand body is close to 400 m/s.

The lower part of the Upper Emilia-Romagna Synthem (AESi), between 85 and 162 m, consists of two transgressive-regressive depositional cycles, separated, at about 127 m, by a transgressive surface. Sea faunae witness delta-marine environments (Minarelli et al., 2016). The trend of natural gamma ray log supports this stratigraphic interpretation. A thin argillaceous layer at about 150 m shows a particularly strong emission, reaching 95 c.p.s. The borehole data show that the stratigraphic unit is associated with a further, gradual increase of the Vs velocity, reaching the maximum value of about 500 m/s at around 145 m, but then decreasing in the lowermost part of the unit, formed by marine muds (Fig. 9).

4.2.2. Lower Emilia-Romagna Synthem (AEI)

The top surface of the synthem was recognized at 162 m, and its base at 292 m. The top discordance can be traced at the regional scale and is locally angular in nature (Petronio et al., 2023). The unit is formed by the intercalation of argillaceous and sand bodies, deposited into marine-deltaic environments and lower alluvial plain settings. Several silty-clay intervals below 210 m contain marine mollusk bioclasts and benthic foraminifera. This interval correlates with nearby marine units, showing infralittoral faunae (Cibin and Segadelli, 2009). Three delta progradation cycles were likely recognized. The fine-grained intercalations show high gamma ray log values, comprising the highest values of the entire well, between 75 and 100 c.p.s., recorded between 180 and 195 m, in an organic-rich mud unit, probably deposited into a coastal marsh. The mud sedimented into more open marine environments, below 265 m, shows lower emission levels. The regional discordance top of the unit is associated with a sharp increase in the Vs to values of more than 500 m/s. Some further Vs peaks are associated with thick sand layers (e.g., 160–170 m and 195–215 m), whereas the fine-grained intervals show lower velocities. The AEI unit contains salty waters enriched in methane (Ferrante et al., 2022), which vented out during drilling, a factor probably influencing the decrease of Vp values observed on borehole data, at depths between 235 and 250 m.

4.2.3. Marine Quaternary (QM1)

A second and sharper discordance surface was reached at 292 m, marking the top of the unit referred to as Marine Quaternary (QM1). The unit is formed by alternating mud and sand layers, sedimented into marine and deltaic environments. The drilling ended at a depth of 380 m, without reaching the QM1 unit base, which is placed at a greater depth, according to the regional stratigraphy framework. The drilled portion of the unit belongs to the upper part of the Lower Pleistocene (Calabrian Stage) and records at least two delta progradation phases, as suggested by the trend of the gamma-ray log and the lithological distribution. The discordance top of the unit is associated with a strong increase in the Vs values in the borehole data, for the first time approaching the value of 800 m/s. Several Vs fluctuations were recorded in the unit, with values always above 500 m/s (Fig. 9). The higher values are associated with sand layers, and the lower ones, between 500 and 600 m/s, were measured in the clay layers. Even in the lowermost portion of the drilled successions, the average Vs values remain well below 800 m/s, which is the threshold defining the engineering bedrock according to both the Italian (NTC18, 2018) and the latest European (CEN, 2022) building codes.

4.2.4. Plio-Pleistocene marine units (QM2 - P2)

The detail and accuracy of the stratigraphic and geophysical interpretation decrease below the layers directly reached by drilling. A characterization of the Plio-Pleistocene units can nevertheless be inferred from Vs estimates obtained through passive surface-wave analysis, supported by prior knowledge of the regional stratigraphy. The interpretation of the deep stratigraphic framework is based on seismic lines and boreholes acquired for hydrocarbon exploration (Ghielmi et al., 2013). A thick Quaternary succession of prodelta and open marine mud is developed to a depth of about 670 m. In nearby areas, this interval was subdivided into upper (QM1) and lower (QM2) Marine Quaternary units, based on their seismic properties (Petronio et al., 2023). In the subsurface of the study site, the boundary between the two QM units is inferred to occur at around 415 m depth, coinciding with the velocity increase identified by the passive surface-wave inversion. The surface-wave passive analysis suggests an average Vs value of about 700 m/s in the QM1 unit. In the underlying QM2 unit, the average Vs values were estimated, from surface-wave inversion, at about 800 m/s, barely reaching the threshold velocity defining the engineering seismic substratum.

Below the Marine Quaternary units, the oldest portion of the discussed succession is developed. The stratigraphic interval is dominated by well lithified sandstones, deposited into deep water marine environments by eastward bound turbidity currents (Inner Porto Garibaldi Fm; Ghielmi et al., 2013). The turbiditic unit is capped by a sedimentation deactivation surface, induced by the tectonic rising of an anticline submarine “dam” in western areas, preventing the turbidite currents from reaching the study area. The turbidite sedimentation was superseded by the slower accumulation of marine clays. Interpretation of passive seismic data indicates that the top of the turbidite unit corresponds to a sharp increase in Vs values, rising by approximately 400 m/s to exceed 1200 m/s (Table 3, Fig. 11). It can be therefore assumed that the upper surface of the turbiditic sandstones corresponds to the top of the seismic substratum.

4.3. Seismic reflectors and resonance frequencies

The geophysical investigations enabled the reconstruction of the shear-wave velocity profile with depth and provided information on the presence of seismic reflectors within the stratigraphic succession. The main sharp increases in velocity identified along the geophysical profiles correspond to the major discontinuity surfaces bounding the stratigraphic units. These surfaces therefore represent seismic reflectors within the stratigraphic succession.

Analysis of down-hole data led to the identification of three main shear-wave (SH) reflectors (red arrows in Fig. 3), inferred from the one-way travel time (twt/2) of polarized shear waves. The upper reflector, I1, has a one-way travel time of 0.60 s and is located at a depth of 163 m; the middle reflector, I2, at 0.73 s and 243 m depth; and the lower reflector, I3, at 0.82 s and 292 m depth (Table 4).

The presence of reflectors were also identified through the interpretation of the S-wave reflection profile acquired at the surface, deriving the velocity from the application of a “semblance” function (Fig. 4) using only the seismic line data. The analysis assumes that the stratigraphic boundaries are planar, horizontal and laterally homogeneous in their petrophysical properties, consistent with the nature of the studied alluvial plain subsurface. The reflection analysis of the surface common source gathered data identifies the same I1 and I2 reflectors. A deeper reflector, likely corresponding to I3, is visible in the surface reflection data (Fig. 4), but it cannot be assigned to a precise depth due

Table 4
List of seismic reflectors identified by SH-wave borehole analysis. For each reflector (I1, I2 and I3), the corresponding one-way travel time, depth (as marked in Fig. 3), and the expected resonance frequency (f_0) calculated using the one-way travel time, are reported. These f_0 values are indicated as vertical bars in the H/V plots of Fig. 10A and Fig. A6 (in Appendix).

SH Reflectors	One-way time (twt/2)	Depth	Expected frequency $f_0 = 1$ / (4 one-way time)	Stratigraphic Surface
I1	0.60 s	163 m	0.42 Hz	Boundary between AES/AEI
I2	0.73 s	243 m	0.34 Hz	Top of deltaic progradational cycle within AEI
I3	0.82 s	292 m	0.30 Hz	Boundary between AEI/QM

to limited offset from the seismic reflection line. Below the depth of 365 m reached in the well, reflector identification was only possible through the surface-wave inversion, suggesting two additional reflectors at ~420 m and ~700 m.

A preliminary estimation of the resonance frequencies (f_0) associated with the three main reflectors identified from SH borehole data (red markers in Fig. 3) was derived using the simple formulation $f_0 = \frac{Vs}{4H} = \frac{1}{2\,twt}$, where *twt* denotes the two-way travel time from the surface to the SH reflector (Table 4).

Once the depth of the three SH reflectors has been established (Fig. 3), the corresponding theoretical frequencies can be directly derived from their *twt*, obtaining values of 0.42, 0.34 and 0.3 Hz (Table 4). These reflectors are consistent with the stratigraphic framework (Fig. 9). The upper reflector (I1) approaches the regional unconformity surface separating the lower (AEI) and upper (AES) synthems. The middle reflector (I2) approximately correlates with the sharp top of the lower deltaic progradational cycle of AEI. The lower reflector (I3) matches the velocity contrast at the top of the Marine Quaternary unit.

The expected frequencies associated with SH reflectors, calculated using the simplified formula (Table 4) can be compared with the frequency peaks observed in the experimental H/V noise spectral ratios curves.

The H/V ratios show fairly consistent curves at the borehole site (Figs.8A and 10A) despite the use of different types of velocimeters and the acquisition at different times (Table 2), even during nighttime, when anthropogenic noise is typically reduced.

The H/V curves derived from the single stations of the 2D array show some differences when compared to those from the borehole site. The 2D array stations show a H/V ratio amplitude larger and a curve trend different from the borehole ones, particularly in the 0.3–0.8 Hz range (Fig. 10B). The H/V array curves show a rightward shift of the descending branch beyond the 0.7 Hz peak, which is more evident than in nighttime recordings and likely indicates a different contribution of body and Love waves to the H/V spectral amplitude (Bonnefoy-Claudet et al., 2008; Endrun, 2011). Similar discrepancies are also observed when comparing the 2D array curves with those derived from the other single-station measurements. The anomalous features observed in the H/V spectral ratios recorded by the array stations were likely driven by anthropogenic, seasonal, and meteorological effects occurring during the acquisition period, influencing even the low-frequency range (< 1 Hz). Similar effects were also described by recent studies in similar geological contexts (Hailemikael et al., 2024; Vassallo et al., 2024; Seivane et al., 2024; El-Hitti et al., 2026).

The spectral curves display three weak peaks at approximately 0.2, 0.35 and 0.7 Hz (Fig. 10A). The peak at 0.7 Hz is the most prominent and therefore it was often wrongly assumed in the literature as the fundamental resonance frequency of the area. The other, lower frequency peaks can be less distinct and recognizable in analogous measurements performed in the region (Mantovani et al., 2019), even when applying the effective identification peak criteria usually employed in ambient vibration analyses (SESAME, 2004; Wang et al., 2023). The peaks identified with the H/V measurements do not always correspond to the frequencies associated with the reflectors, derived from the analysis of active seismic data (Table 4). Such a mismatch may result from the contribution of wave types other than SH waves to the H/V ratios, as well as from the absence of strong impedance contrasts in the subsurface. For instance, reflectors I2 and I3 may not generate distinct spectral signatures in the H/V curve and are likely represented by a single merged peak at about 0.3–0.35 Hz, owing to their limited vertical separation. However, the recurrent observation of the 0.35 and 0.7 Hz H/V peaks across measurements acquired in different seasons and over an extended time span supports their interpretation as stable and persistent seismo-stratigraphic features associated with distinct seismic interfaces. The reflectors identified (Table 4) correspond to major stratigraphic

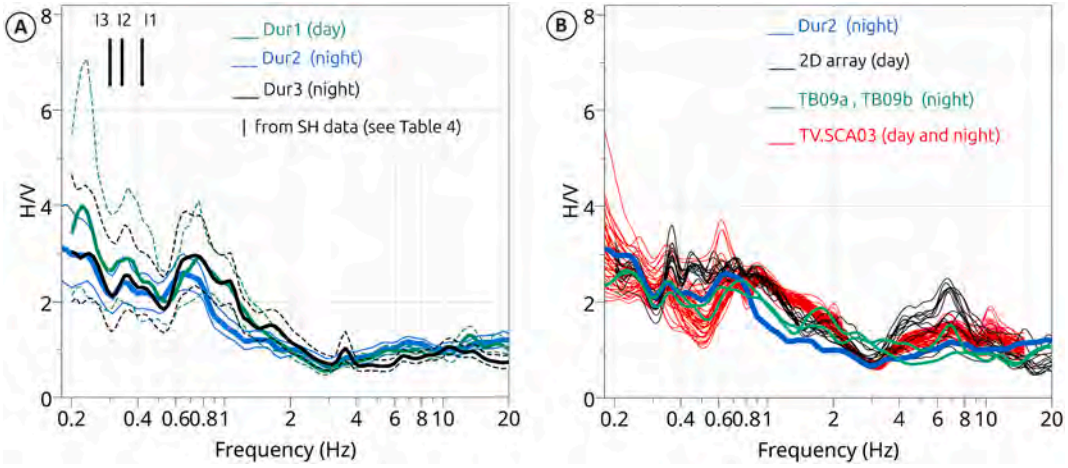

Fig. 10. H/V noise spectral ratios acquired between 2012 and 2025. A) H/V ratios at the borehole site (solid and dashed curves representing mean and ± 1 standard deviation, respectively); colours indicate the date of acquisition (Table 2) with 'day' and 'night' labels distinguishing daytime and nighttime measurements. Vertical bars in the upper left indicate the f_0 values calculated from the SH reflectors (see Table 4). B) Comparison of mean H/V curves from the surrounding sites with the representative curve from the borehole site (Dur2). Red curves show mean H/V ratios (averaged over 24-h) from the TV.SCA03 station (45-day continuous recording). Black curves indicate mean H/V ratios of the individual stations from the 2D array. Green curves depict two additional measurements (TB09a and TB09b performed in 2025). (For interpretation of the references to colour in this figure legend, the reader is referred to the web version of this article.)

surfaces recognized in the borehole data. Reflector I1 is located at a depth of about 163 m and correlates with the boundary between the AES and AEI units. Reflector I2 occurs at the depth of approximately 243 m, associated with the top of a deltaic progradational cycle within the AEI unit. Finally, reflector I3 was identified at a depth of about 292 m, marking the boundary between the AEI and QM units. Below the depth reached by the well, the reflector at about 420 m detected by surface-wave inversion can be correlated with the boundary between the QM1 and QM2 units, recognized within the Marine Quaternary also in a nearby syncline area by seismic reflection data (Petronio et al., 2023). From the regional knowledge of the subsurface, the deepest interface recognized by the inversion analysis at approximately 700 m can be associated with the base of the Marine Quaternary unit, here corresponding to the top of the uppermost Pliocene turbidites (Inner Porto Garibaldi Formation, P2 in Fig. 11). The proposed correlation is in good agreement with the map of the Quaternary Marine unit base depth (Fig. 11), based on a 3-D digital structural model of central Emilia-Romagna (Klin et al., 2019) developed using deep seismic lines and borehole data acquired for hydrocarbon exploration.

Assuming the top of the seismic bedrock at about 700 m depth, the mean shear-wave velocity of unconsolidated deposits above it (Vs_{700}) was computed following the NTC18 prescription as $H/\sum(h_i/V_{si})$. The equivalent shear-wave velocity (Vs_{700}) obtained from the inverted models is 530 m/s, and corresponds to a fundamental frequency of about 0.2 Hz, according to the quarter-wavelength approximation. This frequency is consistent with the H/V resonance peak observed at 0.2 Hz, despite the large uncertainty affecting the H/V curves at this frequency (Fig. 10). Regarding the I1, I2, and I3 reflectors, the quarter-wavelength approximation, using the expected resonant frequencies and the fixed depths reported in Table 4, yields mean Vs values of 274, 330, and 350 m/s, respectively. These values are consistent with the velocity estimations at the depths of the three reflectors (i.e., Vs_{163}, Vs_{243}, and Vs_{292}; Table 4) derived from the power-law relationship proposed above. The resulting mean Vs values are 293, 343, and 369 m/s, respectively. However, as discussed by Dobry et al. (1976), the quarter-wavelength approximation used to estimate the fundamental frequency may become less reliable for deep velocity profiles (Rosenblad and Goetz, 2010; Himel and Wood, 2022).

To overcome the limitations in the f_0 estimation, Rayleigh-wave ellipticity was further compared with the SH-wave transfer function derived from the best-fitting model based on arrays data, as implemented in the Geopsy suite (using *gpell* and *gpsh* codes; Fig. A6 in the Appendix). These are 1D elastic computations requiring quality factors for P and S waves, which, for simplicity, were set equal to 1/10 of Vp and Vs values. The ellipticity modelling is based on the assumptions that ambient vibrations are dominated by surface waves (Maranò et al., 2017), and that the subsurface consists of laterally homogeneous, horizontally layered strata with velocity increasing with depth. Under the assumption of Rayleigh-wave ellipticity, both the deep inversion-based and power-law models yield a Rayleigh peak at approximately 0.4 Hz (Fig. A6 in the Appendix), consistent with the frequency associated with the I1 reflector. The SH transfer function suggests a f_0 value at about 0.3 Hz, close to that associated with the I3 reflector, suggesting a fairly good agreement with the H/V noise curve in the 0.3–0.7 Hz frequency band (Fig. A6). The methods highlight two distinct peaks at frequencies associated with actual seismic reflectors, however not corresponding to the seismic bedrock (Table 4). The SH transfer functions and the ellipticity models are therefore unable to fit the fundamental site resonance at 0.2 Hz, suggesting that a more in-depth analysis is required for assessing the reliability of the 0.2 Hz peak.

Despite their low amplitude, the constant recurrence of the peaks at 0.35 and 0.7 Hz across multiple noise measurements suggests that they may provide valuable constraints on the interpretation of the subsurface model. Although the identification of the site resonance remains challenging in the Po Plain, the consistently observed weak peaks in the H/V spectral ratios at frequencies below 0.7 Hz, particularly the one around 0.35 Hz, appear to be stable and stratigraphically significant.

The 0.7 Hz peak, although not directly associable to the resonance frequency of any SH reflector, is a prominent and persistent feature of the site. Advanced 1D elastic modelling (Fig. A6 in the Appendix) and array processing suggest two possible interpretations for this peak: (i) a secondary resonance in the SH-wave transfer function, which may exhibit multiple amplification maxima in deep, structurally complex basins, or (ii) an effect related to the ellipticity of the first higher

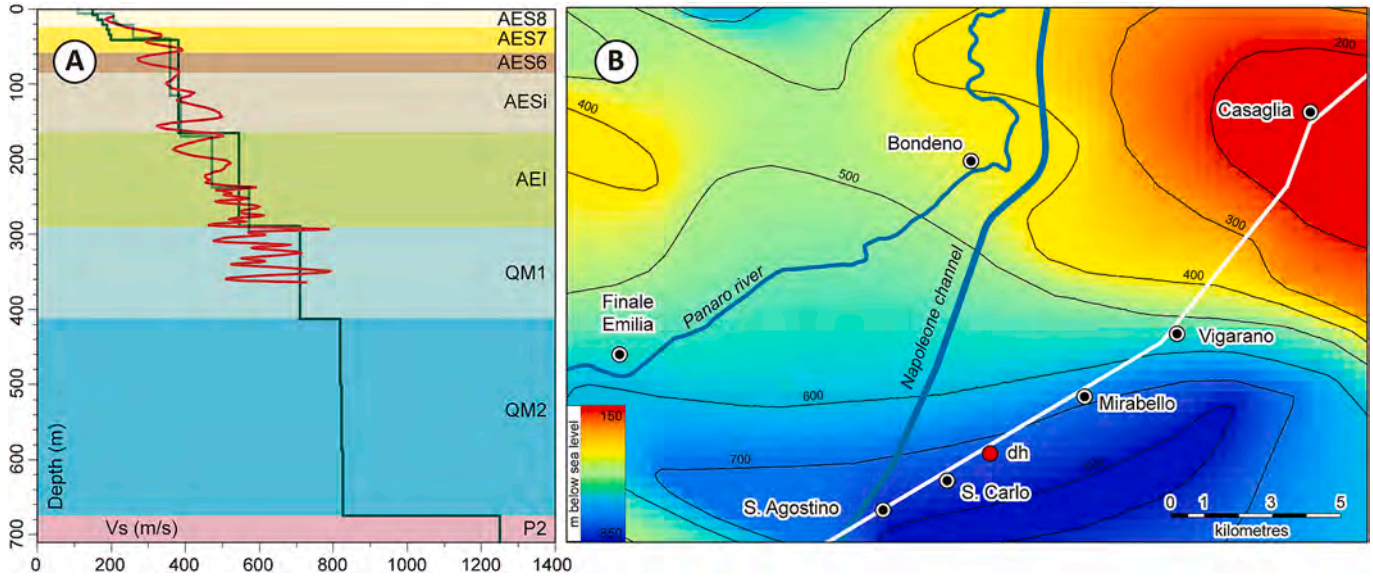

Fig. 11. (A) Correlations between the velocity profiles and the stratigraphic units. The dark green line depicts the best-fitting model from surface-wave inversion, in red the one measured from down-hole, in light green from reflection analysis. Stratigraphic units: AES8 Ravenna Subsynthem, AES7 Villa Verucchio Subsynthem, AES6 Bazzano Subsynthem, AESi lower undifferentiated portion of the Upper Emiliano-Romagnolo Synthem, AEI Lower Emiliano-Romagnolo Synthem, QM1 and QM2 Marine Quaternary units, P2 Porto Garibaldi Fm (seismic bedrock). (B) Map showing the isobaths of the Marine Quaternary base influenced by the tectonic deformation. The white line depicts the trace of the geological profile of Fig. 1. The red dot indicates the study well.

Rayleigh mode (R1), as suggested by the analysis of three-component arrays data. The stability of the 0.7 Hz peak across different measurement campaigns in the region (Milana et al., 2014; Mantovani et al., 2019; Mascandola et al., 2019) suggests that it represents a fundamental seismo-stratigraphic characteristic of this portion of the Po Plain, likely unrelated to the deepest stiff interface, but rather reflecting the combined influence of higher-order wave modes and a weak stiffness contrast within the stratigraphic units.

5. Conclusions

This interdisciplinary study improved the understanding of seismic properties within thick unlithified clayey-sandy units in a synclinal area of the active Apennine foreland basin.

A high-resolution reconstruction of the shear-wave velocity (Vs) profile down to the seismic bedrock was achieved using independent geophysical methods, integrated with detailed well data (cuttings and gamma log) and regional geological correlations. The main findings of this study can be summarized as below:

- Consistent P- and S-wave velocity measurements were obtained from three distinct seismic methods i.e. borehole, surface seismic reflection, and ambient noise array analysis, validating both the acquisition techniques and the resulting velocity models, and a previous borehole survey on the same site (Minarelli et al., 2016).
- Analysis of passive noise array data was essential for extending the seismic interpretation below the well depth, allowing the identification of the deep seismic bedrock. S-wave velocities remain low to considerable depth, with a sharp increase of the velocity exceeding the 800 m/s threshold only around 700 m, at the top of the Pliocene turbidites (Porto Garibaldi Fm.).
- H/V spectral ratios and passive surface-wave methods can provide a robust and cost-effective means of mapping seismic bedrock depth and subsoil velocity structure over wider areas of the Po Plain, provided that their inherently non-unique inversion solutions are constrained and calibrated using stratigraphic information and characteristic velocity ranges of the geological units derived from the study area.
- The observed velocity trends were used to define a power-law function describing the variation of average shear-wave velocity with depth. This function can be used as a reference profile across large portions of the south-western Po Plain, where the stratigraphic features are similar to those of the studied area and deep Vs profiles are commonly lacking.
- High-confidence borehole velocity values were obtained for most of the stratigraphic units of the Quaternary succession. These typical velocity ranges can be used to guide the inversion process of passive data acquired across large portions of the south-western Po Plain, enabling the derivation of more reliable velocity profiles from passive arrays.
- Main seismic reflectors were identified and associated with regional stratigraphic discordances and were tentatively correlated with the observed resonance frequencies.

These results can enhance the understanding of subsurface seismic properties across broader areas of the Apennine foreland basin and in analogous stratigraphic settings. The new knowledge can have significant implications for developing reliable seismic microzonation and site response analyses in seismically active regions. The proper identification of the velocity profiles, and the correct association of the seismic reflectors with their resonance frequency, could largely improve the interpretation of single-station passive data. Accurate interpretation of these data can significantly improve the understanding of the regional seismo-stratigraphic framework, as the use of single-station passive techniques allows the rapid and cost-effective acquisition of a large number of measurements over extensive areas. To further strengthen confidence in the regional relevance of these results, additional studies integrating deep boreholes with both active and passive geophysical techniques at the basin scale should be undertaken.

CRediT authorship contribution statement

Giuseppe Di Giulio: Writing – review & editing, Writing – original draft, Supervision, Methodology, Investigation, Formal analysis, Data curation, Conceptualization. **Marco Stefani:** Writing – review & editing, Writing – original draft, Supervision, Methodology, Formal analysis, Conceptualization. **Giuliano Milana:** Writing – review & editing, Supervision, Methodology, Investigation, Funding acquisition, Formal analysis, Conceptualization. **Maurizio Vassallo:** Writing – review & editing, Investigation, Data curation. **Sara Amoroso:** Writing – review & editing, Investigation. **Gabriele Tarabusi:** Writing – review & editing, Supervision. **Luca Baradello:** Writing – review & editing, Investigation, Data curation. **Alessandro Affatato:** Investigation, Data curation. **Alfio Barbagallo:** Investigation, Data curation. **Stefano Maffione:** Investigation, Data curation. **Lorenzo Petronio:** Writing – original draft, Supervision, Methodology, Investigation, Funding acquisition, Formal analysis, Data curation, Conceptualization. **Luca Minarelli:** Writing – review & editing, Writing – original draft, Supervision, Methodology, Investigation, Formal analysis, Data curation, Conceptualization.

Declaration of competing interest

The authors declare that they have no known competing financial interests or personal relationships that could have appeared to influence the work reported in this paper.

Acknowledgments

We thank the Esito Laboratory of INGV (https://www.ingv.it/en/monitoraggio-e-infrastrutture/laboratori/laboratorio-effetti-di-sito) to support with seismic equipment the field measurements performed by INGV team. We thank Regione Veneto for providing us the profile of gamma-ray log. This work was in part financially supported by 'MIUR-FIRB Abruzzo' Project (UR); PRIN-SERENA 2022-24 'WP6 Mapping Seismic Site Effects at regional and national scale', and 'CARG-Ferrara' Project.

Lorenzo Petronio passed away before the paper was published. This work is dedicated to him with affection and regret.

Appendix A. Supplementary data

Supplementary data to this article can be found online at https://doi.org/10.1016/j.enggeo.2026.109133.

Data availability

INGV row data that support the findings of this study are available from the corresponding author upon reasonable request. OGS data not available due to legal restrictions. The velocity values for P and S velocities are indicated in Tables S2 and S3.

References

Aki, K., 1957. Space and time spectra of stationary stochastic waves, with special reference to microtremors. Bull. Earthq. Res. Inst. Tokyo 35, 415–457.

Arai, H., Tokimatsu, K., 2005. S-wave velocity profiling by joint inversion of microtremor dispersion curve and horizontal-to-vertical (H/V) spectrum. Bull. Seismol. Soc. Am. 95 (5), 1766–1778.

Bard, P.Y., Bouchon, M., 1985. The two-dimensional resonance of sediment-filled valleys. Bull. Seismol. Soc. Am. 75 (2), 519–541.

Bettig, B., Bard, P.Y., Scherbaum, F., Riepl, J., Cotton, F., Cornou, C., Hatzfeld, D., 2001. Analysis of dense array noise measurements using the modified spatial auto-correlation method (SPAC): application to the Grenoble area. Boll. Geofis. Teor. Appl. 42 (3–4), 281–304.

Bonnefoy-Claudet, S., Cornou, C., Bard, P.Y., Cotton, F., Moczo, P., Kristek, J., Fäh, D., 2006. H/V ratio: a tool array noise measurements using the modified spatial auto-correlation method (SPAC): application to the Grenoble area. Bollettino di Geofisica Teorica ed Applicata 42(3-4), pp.281-304.For site effects evaluation. Results from 1-D noise simulations. Geophys. J. Int. 167 (2), 827–837.
Bonnefoy-Claudet, S., Köhler, A., Cornou, C., Wathelet, M., Bard, P.Y., 2008. Effects of love waves on microtremor H/V ratio. Bull. Seismol. Soc. Am. 98 (1), 288–300.
Boore, D.M., Asten, M.W., 2008. Comparisons of shear-wave slowness in the Santa Clara Valley, California, using blind interpretations of data from invasive and noninvasive methods. Bull. Seismol. Soc. Am. 98 (4), 1983–2003.
Caputo, R., Poli, M.E., Minarelli, L., Rapti, D., Sboras, S., Stefani, M., Zanferrari, A., 2016. Palaeoseismological evidence for the 1570 Ferrara earthquake, Italy. Tectonics 35, 1423–1445. https://doi.org/10.1002/2016TC004238.
CEN, 2022. prEN 1998-1-1: Eurocode 8: Design of Structures for Earthquake Resistance - Part 1–1: General Rules and Seismic Actions. European Committee for Standardization, Brussels, Belgium.
Cibin, U., Segadelli, S., 2009. Note Illustrative Della Carta Geologica d'Italia Alla Scala 1: 50,000, Foglio 203, Poggio Renatico. Servizio Geologico d'Italia, Rome, p. 104.
Comina, C., Di Chiara, G., Foti, S., 2023. On the direct estimation of bedrock depth and time-weighted average VS from surface waves dispersion and HVSR curves. J. Appl. Geophys. 215, 105086.
Deschenes, M.R., Wood, C.M., Wotherspoon, L.M., Bradley, B.A., Thomson, E., 2018. Development of deep shear wave velocity profiles in the Canterbury Plains, New Zealand. Earthquake Spectra 34 (3), 1065–1089.
Dix, C.H., 1955. Seismic velocities from surface measurements. Geophysics 20, 68–86. https://doi.org/10.1190/1.1438126.
Dobry, R., Oweis, I., Urzua, A., 1976. Simplified procedures for estimating the fundamental period of a soil profile. Bull. Seismol. Soc. Am. 66 (4), 1293–1321.
Dujardin, A., Causse, M., Courboulex, F., Traversa, P., 2016. Simulation of the basin effects in the Po Plain during the Emilia-Romagna seismic sequence (2012) using empirical Green's functions. Pure Appl. Geophys. 173, 1993–2010.
El-Hitti, J., Gélis, C., Régnier, J., Lenti, L., Cultrera, G., Di Giulio, G., Minarelli, L., Langlaude, P., Pernoud, M., Bustos, J., Schibuola, A., Riccio, G., 2026. Dense geophysical measurements to assess 1D Vs profile of a liquefiable site in the Po Plain (Italy). Eng. Geol. https://doi.org/10.1016/j.enggeo.2026.109075.
Endrun, B., 2011. Love wave contribution to the ambient vibration H/V amplitude peak observed with array measurements. J. Seismol. 15 (3), 443–472.
Ferrante, G.M., Donda, F., Volpi, V., Tinivella, U., Adelinet, M., 2022. Methane occurrence and quantification in a very shallow water environment: a multidisciplinary approach. Geochem. Geophys. Geosyst. 23 (3), e2021GC010276.
Finney, S., 2010. Formal definition of the Quaternary system/period and redefinition of the Pleistocene series/epoch. Episodes 33 (3), 159–163. https://doi.org/10.18814/epiiugs/2010/v33i3/003.
Garofalo, F., Foti, S., Hollender, F., Bard, P.Y., Cornou, C., Cox, B.R., Ohrnberger, M., Sicilia, D., Asten, M., Di Giulio, G., et al., 2016. InterPACIFIC project: comparison of invasive and non-invasive methods for seismic site characterization. Part I: intra-comparison of surface wave methods. Soil Dyn. Earthq. Eng. 82, 222–240.
Ghielmi, M., Minervini, M., Nini, C., Rogledi, S., Rossi, M., 2013. Late Miocene–Middle Pleistocene sequences in the Po Plain – Northern Adriatic Sea (Italy): the stratigraphic record of modification phases affecting a complex foreland basin. Mar. Pet. Geol. 42, 50–81. ISSN 0264-8172. https://doi.org/10.1016/j.marpetgeo.2012.11.007.
Giallini, S., Sirianni, P., Pagliaroli, A., Pizzi, A., Mancini, M., Kaiser, A., Bourguignon, S., Bruce, Z., Hill, M., Liam Wotherspoon, L., Moscatelli, M., 2024. Reconstruction of a subsoil model for local seismic response evaluation through experimental and numerical methods: the case of the Wellington CBD, New Zealand. Eng. Geol. 330, 107413.
Godio, A., Strobbia, C., 2007. Analysis of borehole guided waves for geotechnical application. Boll. Geofis. Teor. Appl. 48 (2), 185–204.
Gupta, S.V., Parvez, I.A., Khan, P.K., 2023. Site response analysis beneath the Kashmir basin (NW Himalaya) using ambient noise. Earthquake Spectra 39 (4), 2436–2469. https://doi.org/10.1177/87552930231195640.
Hailemikael, S., Vassallo, M., Mercuri, A., et al., 2024. In: HVSR analysis of nodal array seismic data acquired in the Fucino Basin (Central Italy). 39th General Assembly of the European Seismological Commission, ESC2024, 22–27 September 2024, Corfù, Greece.
Himel, A.K., Wood, C.M., 2021. Developing an updated set of Vs profiles for the Central United States seismic observatory with estimates of uncertainty between different methods. Soil Dyn. Earthq. Eng. 143, 106594.
Himel, A.K., Wood, C.M., 2022. Deep shear wave velocity profiles in the Mississippi embayment from surface wave measurements. Soil Dyn. Earthq. Eng. 158, 107293.
Hunter, J.A., Benjumea, B., Harris, J.B., Miller, R.D., Pullan, S.E., Burns, R.A., Good, R.L., 2002. Surface and downhole shear wave seismic methods for thick soil site investigations. Soil Dyn. Earthq. Eng. 22 (9–12), 931–941.
Ibs-von Seht, M., Wohlenberg, J., 1999. Microtremor measurements used to map thickness of soft sediments. Bull. Seismol. Soc. Am. 89 (1), 250–259.
Kagawa, T., Zhao, B., Miyakoshi, K., Irikura, K., 2004. Modeling of 3D basin structures for seismic wave simulations based on available information on the target area: case study of the Osaka basin, Japan. Bull. Seismol. Soc. Am. 94 (4), 1353–1368.
Klin, P., Laurenzano, G., Romano, M.A., Priolo, E., Martelli, L., 2019. ER3D: a structural and geophysical 3-D model of Central Emilia-Romagna (northern Italy) for numerical simulation of earthquake ground motion. Solid Earth 10, 931–949. https://doi.org/10.5194/se-10-931-2019.
Lanzano, G., D'Amico, M., Felicetta, C., Puglia, R., Luzi, L., Pacor, F., Bindi, D., 2016. Ground-motion prediction equations for region specific probabilistic seismic-hazard analysis. Bull. Seismol. Soc. Am. 106 (1), 73–92.
Louie, J.N., Pancha, A., Kissane, B., 2022. Guidelines and pitfalls of refraction microtremor surveys. J. Seismol. 1–16.
Mantovani, A., Abu Zeid, N., Bignardi, S., Tarabusi, G., Santarato, G., Caputo, R., 2019. Seismic noise-based strategies for emphasizing recent tectonic activity and local site effects: the Ferrara Arc, Northern Italy, case study. Pure Appl. Geophys. 176 (6), 2321–2347. https://doi.org/10.1007/s00024-019-02120-8.
Maranò, S., Hobiger, M., Fäh, D., 2017. Retrieval of Rayleigh wave ellipticity from ambient vibration recordings. Geophys. J. Int. 209 (1), 334–352.
Martelli, L., 2021. Assessment of seismic bedrock in deep alluvial plains. Case studies from the Emilia-Romagna Plain. Geosciences 11 (7), 297.
Martelli, L., Bonini, M., Calabrese, L., Corti, G., Ercolessi, G., Molinari, F.C., Piccardi, L., Pondrelli, S., Sani, F., Severi, P., 2016. Carta Sismotettonica della Regione Emilia-Romagna e Aree limitrofe, scala 1:250.000 (Edizione 2016). Regione Emilia-Romagna- SGSS, CNR-IGG sez. FI, Università degli Studi di Firenze-DST, INGV sez. BO. D.R.E.AM. Italia.
Mascandola, C., Barani, S., Albarello, D., 2023. Impact of site-response characterization on probabilistic seismic hazard in the Po plain (Italy). Bull. Seismol. Soc. Am. https://doi.org/10.1785/0120220177.
Mascandola, C., Barani, S., Massa, M., Albarello, D., 2021. New insights into long-period (> 1 s) seismic amplification effects in deep sedimentary basins: a case of the Po Plain basin of northern Italy. Bull. Seismol. Soc. Am. 111 (4), 2071–2086.
Mascandola, C., Massa, M., Barani, S., Albarello, D., Lovati, S., Martelli, L., Poggi, V., 2019. Mapping the seismic bedrock of the Po Plain (Italy) through ambient-vibration monitoring. Bull. Seismol. Soc. Am. 109 (1), 164–177.
Massa, M., Lovati, S., Puglia, R., Brunelli, G., Lorenzetti, A., Mascandola, C., Felicetta, C., Pacor, F., Luzi, L., 2022. Seismo-stratigraphic model for the urban area of Milan (Italy) by ambient vibration monitoring and implications for seismic site effects assessment. Front. Earth Sci. 10, 915083. https://doi.org/10.3389/feart.2022.915083.
Matsushima, S., Kosaka, H., Kawase, H., 2017. Directionally dependent horizontal-to-vertical spectral ratios of microtremors at Onahama, Fukushima, Japan. Earth Planets Space 69 (1), 96.
Matsushima, S., Yamanaka, H., Tsuno, S., Chimoto, K., Suzuki, H., Kawase, H., Matsushima, T., 2024. Investigation of the subsurface structure at the target site in Kumamoto, Japan, and the distributed data of the blind prediction exercise: report for the experiments for the 6th international symposium on effects of surface geology on seismic motion. Earth Planets Space 76 (1), 43.
Milana, G., Bordoni, P., Cara, F., Di Giulio, G., Hailemikael, S., Rovelli, A., 2014. 1D velocity structure of the Po River plain (Northern Italy) assessed by combining strong motion and ambient noise data. Bull. Earthq. Eng. 12, 2195–2209.
Minarelli, L., Amoroso, S., Tarabusi, G., Stefani, M., Pulelli, G., 2016. Down-hole geophysical characterization of middle-upper Quaternary sequences in the Apennine Foredeep, Mirabello, Italy. Ann. Geophys. 59 (5), S0543. https://doi.org/10.4401/ag-7114.
Molinari, I., Argnani, A., Morelli, A., Basini, P., 2015. Development and testing of a 3D seismic velocity model of the Po Plain sedimentary basin, Italy. Bull. Seismol. Soc. Am. 105 (2A), 753–764.
Molnar, S., Sirohey, A., Assaf, J., Bard, P.Y., Castellaro, S., Cornou, C., Cox, B., Guillier, B., Hassani, B., Kawase, H., Matsushima, S., 2022. A review of the microtremor horizontal-to-vertical spectral ratio (MHVSR) method. J. Seismol. 1–33.
Mulargia, F., Castellaro, S., 2016. HVSR deep mapping tested down to~ 1.8 km in Po Plane Valley, Italy. Phys. Earth Planet. Inter. 261, 17–23.
Nakamura, Y., 2019. What is the Nakamura method? Seismol. Res. Lett. 90 (4), 1437–1443.
NTC18, 2018. Ministero delle Infrastrutture e dei Trasporti. In: Decreto 17 gennaio 2018. Aggiornamento delle Norme Tecniche per le Costruzioni, G.U., Italian, 2018, no. 42.
Ohori, M., Nobata, A., Wakamatsu, K., 2002. A comparison of ESAC and FK methods of estimating phase velocity using arbitrarily shaped microtremor analysis. Bull. Seismol. Soc. Am. 92, 2323–2332.
Ohta, Y., Goto, N., Yamamizu, F., Takahashi, H., 1980. S-wave velocity measurements in deep soil deposit and bedrock by means of an elaborated down-hole method. Bull. Seismol. Soc. Am. 70 (1), 363–377.
Okada, H., 2006. Theory of efficient array observations of microtremors with special reference to the SPAC method. Explor. Geophys. 37 (1), 73–85.
Park, C.B., Miller, R.D., Xia, J., 1999. Multichannel analysis of surface waves. Geophysics 64 (3), 800–808.
Petronio, L., Baradello, L., Poggi, V., Minarelli, L., Böhm, G., Affatato, A., Barbagallo, A., Cristofano, G., Sorgo, D., Martelli, L., Lai, C.G., 2023. Combining SH-and P-wave seismic reflection survey to support seismic response analysis. A case study from Cavezzo (Italy) after the 2012 Emilia earthquake. Eng. Geol. 313, 106916. https://doi.org/10.1016/j.enggeo.2022.106916.
Pieri, M., Groppi, G., 1981. Subsurface Geological Structure of the Po Plain, vol. 414. Italy. Pubbl, pp. 1–11.
Pondrelli, S., Salimbeni, S., Perfetti, P., Danecek, P., 2012. Quick regional centroid moment tensor solutions for the Emilia 2012 (northern Italy) seismic sequence. Ann. Geophys. 55 (4), 615–621. https://doi.org/10.4401/ag-6146.
Regione Emilia-Romagna, 1998. In: Di Dio, G.M. (Ed.), ENI Agip Divisione Esplorazione e Produzione. Riserve Idriche Sotterranee della Regione Emilia-Romagna. S.EL.CA, Firenze, Italy, p. 120.
Riga, E., Makra, K., Pitilakis, K., 2016. Aggravation factors for seismic response of sedimentary basins: a code-oriented parametric study. Soil Dyn. Earthq. Eng. 91, 116–132.
Rosenblad, B.L., Bailey, J., Csontos, R., Van Arsdale, R., 2010. Shear wave velocities of Mississippi embayment soils from low frequency surface wave measurements. Soil Dyn. Earthq. Eng. 30 (8), 691–701.

Rosenblad, B.L., Goetz, R., 2010. Study of the H/V spectral ratio method for determining average shear wave velocities in the Mississippi embayment. Eng. Geol. 112 (1–4), 13–20.

Seivane, H., Schimmel, M., Martí, D., Sánchez-Pastor, P., 2024. Rayleigh wave ellipticity from ambient noise: a practical method for monitoring seismic velocity variations in the near-surface. Eng. Geol., 107768 https://doi.org/10.1016/j.enggeo.2024.107768.

SESAME team, 2004. Guidelines for the Implementation of the H/V Spectral Ratio Technique on Ambient Vibrations: Measurements, Processing and Interpretation (Deliverable No. D23.12), WP12. SESAME European research project. https://sesame.geopsy.org/Delivrables/Del-D23-HV_User_Guidelines.pdf (last access April 2025).

Stefani, M., Minarelli, L., Fontana, A., Hajdas, I., 2018. Regional deformation of late Quaternary fluvial sediments in the Apennines foreland basin (Emilia, Italy). Int. J. Earth Sci. 107 (7), 2433–2447. https://doi.org/10.1007/s00531-018-1606-x.

Stephenson, W.J., Louie, J.N., Pullammanappallil, S., Williams, R.A., Odum, J.K., 2005. Blind shear-wave velocity comparison of ReMi and MASW results with boreholes to 200 m in Santa Clara Valley: implications for earthquake ground motion assessment. Bull. Seismol. Soc. Am. 95 (6), 2506–2516.

Tarabusi, G., Sgattoni, G., Caputo, R., 2024. Imaging buried anticlines in the Po Plain, northern Italy, based on HVSR frequency and amplitude analyses. Int. J. Earth Sci. 113 (6), 1457–1473.

Teague, D., Cox, B., Bradley, B., Wotherspoon, L., 2018. Development of deep shear wave velocity profiles with estimates of uncertainty in the complex interbedded geology of Christchurch, New Zealand. Earthquake Spectra 34 (2), 639–672.

Vannoli, P., Burrato, P., Valensise, G., 2015. The seismotectonics of the Po Plain (northern Italy): Tectonic diversity in a blind faulting domain. Pure Appl. Geophys. 172, 1105–1142.

Vassallo, M., Cultrera, G., Esposito, A., Mercuri, A., Bobbio, A., Di Giulio, G., Milana, G., Bordoni, P., Ciaccio, M.G., Cara, F., 2024. Temporary Seismic Network in the Metropolitan Area of Rome (Italy): New Insight on an Urban Seismology Experiment. Seismol. Res. Lett. 95, 2554–2569. https://doi.org/10.1785/0220230290.

Vassallo, M., Riccio, G., Mercuri, A., Cultrera, G., Di Giulio, G., 2023. HV noise and earthquake automatic analysis (HVNEA). Seismol. Res. Lett. 94 (1), 350–368.

Wang, P., Zimmaro, P., Ahdi, SK., Yong, A. and Stewart J.P., 2023. Identification protocols for horizontal-to-vertical spectral ratio peaks. Bull. Seismol. Soc. Am. (1; 113(2):782-803).

Wathelet, M., Chatelain, J.L., Cornou, C., Di Giulio, G., Guillier, B., Ohrnberger, M., Savvaidis, A., 2020. Geopsy: a user-friendly open-source tool set for ambient vibration processing. Seismol. Res. Lett. 91 (3), 1878–1889.

Wathelet, M., Guillier, B., Roux, P., Cornou, C., Ohrnberger, M., 2018. Rayleigh wave three-component beamforming: signed ellipticity assessment from high-resolution frequency-wavenumber processing of ambient vibration arrays. Geophys. J. Int. 215 (1), 507–523.

Woolery, E.W., Wang, Z., Seth Carpenter, N., Street, R., Brengman, C., 2016. The Central United States seismic observatory: site characterization, instrumentation, and recordings. Seismol. Res. Lett. 87 (1), 215–228.